U. S. Department of Commerce
National Oceanic and Atmospheric Administration
National Weather Service
National Centers for Environmental Prediction
5200 Auth Road Room 207
Camp Springs, MD 20746

Technical Note

A review of operational forecasting of wind generated waves by hurricane Isabel at NCEP. [†]

Hendrik L. Tolman [‡,♯], Jose Henrique G. M. Alves [♯], and Yung Y. Chao

Environmental Modeling Center
Marine Modeling and Analysis Branch

January 2004

[†] MMAB Contribution No. 235.

[‡] e-mail: Hendrik.Tolman@NOAA.gov

[♯] Science Applications International Corporation / GSO

This page is intentionally left blank.

Abstract

The accuracies of the operational wave models at the National Centers for Environmental Prediction (NCEP) for sea states generated by hurricane Isabel are assessed. The Western North Atlantic (WNA) and the North Atlantic Hurricane (NAH) wave models are validated using analyzed wind fields, and wave observations from the Jason-1 satellite borne altimeter and from 15 moored buoys. Both models provided excellent guidance for Isabel in the days preceding landfall of the hurricane on the east coast of the USA. However, the NAH model outperforms the WNA model in the initial stages of Isabel, when Isabel was a category 5 hurricane. The NAH model was also more accurate in providing guidance for the swell systems arriving at the US coast well before landfall of Isabel. Although most model deficiencies can be attributed to shortcomings in the driving wind fields, several areas of potential wave model improvement have been identified. These are: (i) shallow water behavior on the southern Atlantic shelf, (ii) the physical parameterizations in extreme wind conditions, (iii) the inclusion of wave-current interaction due to both tides and the Gulf Stream, and (iv) several numerical issues.

Acknowledgments. The authors like to thank NDBC, in particular Dave Gilhousen and Richard Bouchard, and AOML, in particular Mark Powell, for their help with obtaining validation data and background information relevant for these data. We also would like to thank D.B. Rao for his comments on early drafts of this manuscript.

This report is available as a pdf file from

http://polar.ncep.noaa.gov/waves

Contents

This page is intentionally left blank.

1 Introduction

Hurricane Isabel ravaged the east coast of the United States in September 2003. Due to the size and intensity of this hurricane, extreme wave conditions were observed and predicted along the coast. Significant wave heights greater than 10 m were observed about 250 nm offshore at National Data Buoy Center (NDBC) buoys 41001 and 41002, which were located on either side of the corridor of predicted maximum wave heights. NDBC buoy 41025, located right in the path of predicted maximum wave heights, was rendered inoperative well before the most extreme wave conditions were reached. The operational wave models at NCEP predicted wave height at this buoy up to 15 m. Considering that the mean water depth at this buoy is only 19 m, it is not surprising that the buoy was lost. This buoy was later found by the Coast Guard beached in shallow water in Pamlico Sound, with severe damage (Dave Gilhousen, NDBC, personal communication). Extreme wave conditions extended up to the coast. At a waverider buoy only 2 nm offshore at the Field Research Facility (FRF) of the US Army Corps of Engineers at Duck, NC[1], wave heights of up to 8.1 m were observed.

In this paper we review the performance of the guidance forecasts produced by the operational wind wave models for the western north Atlantic Ocean domain at the National Centers for Environmental Prediction (NCEP) during the life cycle of hurricane Isabel. NCEP has provided numerical wind wave guidance for several decades (see Tolman et al., 2002). Presently, the suite of operational wave models at NCEP consists of a global model with a spatial resolution of $1^\circ \times 1.25^\circ$ in latitude and longitude, and several regional models with a spatial resolution of typically 0.25°. This set of models is know as the NOAA WAVEWATCH III model suite. A detailed description of parts of the model suite as relevant for the present study can be found in Tolman et al. (2002), Tolman (2002a,c), (Chen et al., 2003), and Chao et al. (2003a,b).

Most wave models at NCEP are forced with analysis and forecast winds generated by the Global Forecasting System (GFS) model (see, for example, Caplan et al., 1997; Moorthi et al., 2001). However, global weather forecast models such as the GFS generally do not have sufficient resolution to accurately describe hurricanes, and may even lack the proper physical parameterizations. For this reason, a separate hurricane wave prediction model, the North Atlantic Hurricane wave model (NAH) has been implemented in addition to the regular Western North Atlantic regional wave model (WNA) and the global wave model (NWW3). The NAH wave model differs from the WNA and NWW3 models, in that it uses high resolution wind fields from operational hurricane wind models near hurricanes (see Section 2). Because the resolution of the global NWW3 model is insufficent to resolve the characteristic waves generated by hurricanes with small spatial scales, only the WNA and NAH models will be considered in this study.

[1] see http://www.frf.usace.army.mil

The present paper addresses the accuracy of operational hurricane wave predictions at NCEP for hurricane Isabel. In Section 2, the wave models and the validation data are described. Because the accuracy of wave forecasts is heavily dependent on the quality of the driving wind fields, the accuracy of wind fields is assessed in section 3, before model wave height predictions are compared with buoy and altimeter data in Section 4. In Section 5 a more in-depth spectral analysis is presented for several buoy locations. A discussion and conclusions are presented in Sections 6 and 7, respectively.

2 Models and data

Three operational wave prediction models produced guidance for the north Atlantic Ocean during the life cycle of hurricane Isabel. These were the global NOAA WAVEWATCH III (NWW3) model, the Western North Atlantic regional model (WNA) and the North Atlantic Hurricane regional wave model (NAH). As mentioned earlier, we will not consider the global NWW3 model here. The present WNA and NAH models are based on version 2.22 of the WAVEWATCH III model (Tolman, 2002a,c; Tolman et al., 2002). These implementations of WAVEWATCH III use the default model setting as defined in Tolman (2002c) with few exceptions. Details of the model setup, including modifications relative to the default settings of WAVEWATCH III, are shown in Table 2.1.

Input for the wave model consists of near-surface wind fields and ice concentration fields. The latter are obtained from NCEP's automated passive microwave sea ice concentration analysis (Grumbine, 1996) and are updated daily. Wind fields are generally provided by NCEP's Global Forecast System (GFS), mentioned earlier. These are available at three hour intervals and presently have a spectral resolution of T254. For the NAH wave model, high resolution wind fields, generated hourly at NCEP by the Geophysical Fluid Dynamics Laboratory (GFDL) model for individual hurricanes, are blended with 3-hourly GFS wind fields. For this purpose, hourly GFS wind fields are generated by interpolation. The blending scheme is described in detail in Chao and Tolman (2000, 2001) and Chao et al. (2004).

The quality of these different wind fields is assessed using independent analyses of surface winds for Isabel from the Hurricane Research Division (HRD) of the Atlantic Oceanographic and Meteorological Laboratory (AOML) of NOAA (Powell et al., 1996, 1998). All data used here have been obtained from the HRD web site[2]. Best track information was obtained from the advisories of NCEP's Tropical Prediction Center (TPC)[3].

Traditionally, wave models are validated using data from buoys. In the present study, we use the data from NDBC for buoy locations shown in Fig. 2.1. Although these data are received at NCEP in near real time as part of the operational data stream, quality controlled data can also be obtained from the NDBC web site[4]. We have used the latter data for the present study.

Buoy data are generally available near most coastal areas of the USA, but generally do not cover the deep ocean well. Global wave height data for deep water locations may, however, be obtained from altimeters on board satellites. At the time of Isabel, altimeter data were available from the Jason-1 satellite. The Jason-1 data used here were retrieved from the historical archive at the

[2] http://www.aoml.noaa.gov/hrd

[3] Composite from http://weather.unisys.com/hurricane/atlantic/2003/index.html

[4] http://www.ndbc.noaa.gov

Table 2.1: Implementation details of the operational WAVEWATCH III models for the North Atlantic Ocean at NCEP. The nonstandard options are namelists as used in the input file of the ww3_grid component of WAVEWATCH. $d_{\min}$ is the smallest water depth allowed in the model.

Model	Grid	$d_{\min}$ (m)	Nonstandard WAVEWATCH III options
WNA	0°- 50°N	7.5	&sbt1 gamma = -0.019 /
	98°-30°W		&misc flagtr = 4, cice0 = 0.25, cicen = 0.75 /
	0.25°×0.25°		
NAH	0°- 50°W	7.5	&sbt1 gamma = -0.019 /
	98°-30°W		&misc flagtr = 4, cice0 = 0.25, cicen = 0.75 /
	0.25°×0.25°		&pro3 wdthcg = 2.00, wdthth = 2.00 /

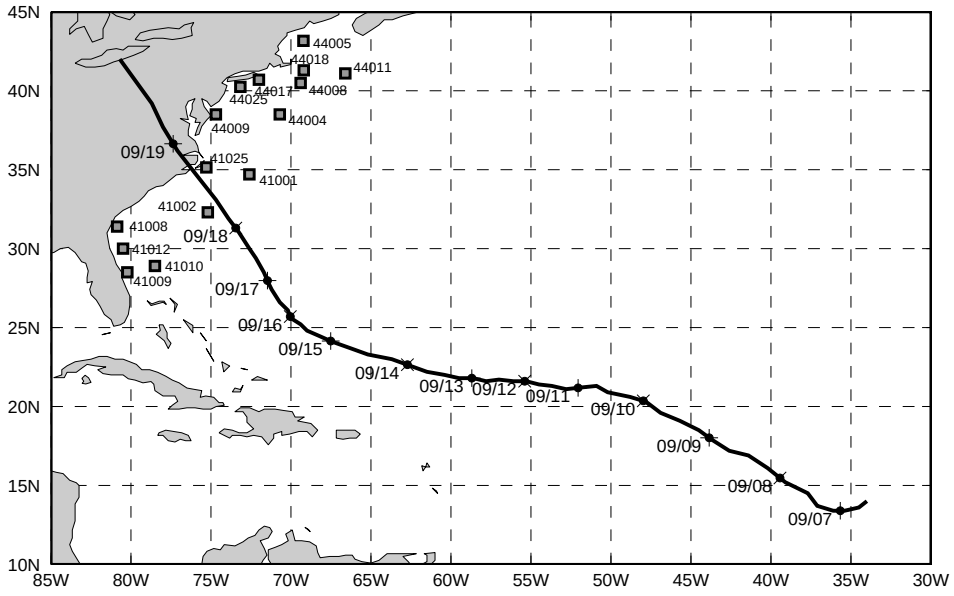

Fig. 2.1 : Buoy locations used in this study and the best guess track of hurricane Isabel. Dates along track correspond to 0000 UTC.

Naval Research Laboratory (NRL), through their web[5] and ftp[6] servers. All buoy and altimeter data are used here at their original resolution, that is, without additional averaging, except for the spectral buoy data used in Section 5.

[5] http://www7320.nrlssc.navy.mil
[6] ftp://ftp7320.nrlssc.navy.mil

This page is intentionally left blank.

3 Isabel's surface wind fields

TPC first identified Isabel in an advisory issued 1300 UTC on September 6, 2003. At this time Isabel was identified as a tropical storm with the center near 14°N and 34°W, moving to the west with a speed of 11 kt. The complete track of Isabel over water is shown in Fig. 2.1. This Figure also gives an impression of the hurricane's forward speed. According to advisories published subsequently by TPC [7], at 1500 UTC September 7, Isabel had become a category 1 hurricane. Over the next few days Isabel gradually gained strength, reaching category 5 status at 2100 UTC on September 11 with maximum sustained winds of 140 kt. Isabel retained this strength through early September 15. Thereafter it gradually weakened, dropping to category 2 strength with sustained winds of 90 kt on 1500 UTC September 16. Through landfall on early September 19, Isabel retained this strength.

The quality of the wind fields used to drive the WNA and NAH wave models during Isabel's lifetime is assessed in several ways. First, analyzed wind fields from the NAH and WNA models (GFDL wind fields from the shortest range forecast available, and analyses from GFS, respectively) are compared with the analyses performed by AOML. Selected examples are given in Fig. 3.1. The intensity of Isabel in the WNA and NAH models is assessed by comparing maximum wind speeds in both models with the maximum wind speed from the AOML analyses in Fig. 3.2. Forecast tracks of Isabel are compared to the best track estimate from TPC in Fig. 3.3.

The AOML analyses are produced interactively, requiring human intervention. Generally, they are available for hurricanes at six hour intervals, but not always at fixed times. From the AOML website, we have downloaded 25 analyses of Isabel's surface winds, starting at 1730 UTC on September 11, and ending near landfall at 1630 UTC, September 18. Thus, no AOML data are available for the initial stages of Isabel, and she is already a category 5 hurricane when the first AOML data have become available.

We will first address the quality of the analyzed wind fields, as used in the hindcasts of the wave models. These represent the best wind fields available, and therefore tentatively provide an upper bound for the accuracy of the wave model system. Furthermore, swells sufficiently far away from the center of Isabel are generated solely by these analyzed winds. Hence, the quality of the analyzed wind fields is of paramount importance for the swell forecasts at the buoy locations before Isabel comes close to land.

While Isabel was a category 5 hurricane (September 12 and 13), the NAH (GFDL) model generally captured the structure of the wind field well, but wind speeds were generally lower than the AOML data (Fig. 3.2). The WNA (GFS) winds were much weaker than the NAH and AOML winds (Fig. 3.2), and the

[7] http://www.nhc.noaa.gov/archive/2003/ISABEL.shtml?

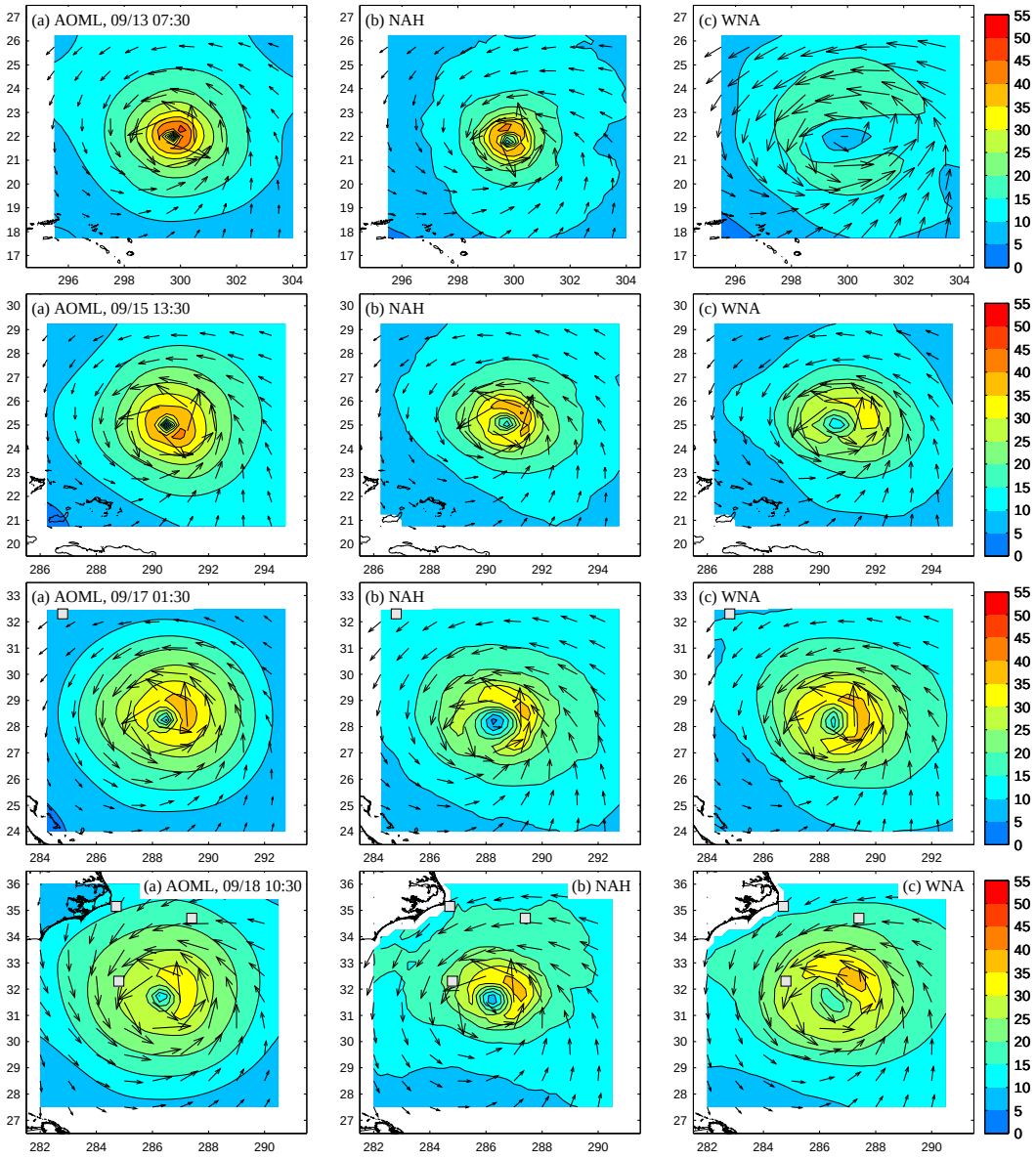

Fig. 3.1 : Wind speeds at 10 m height in $ms^{-1}$for Isabel from the AOML analysis (panel a, 10 min average wind speeds), the NAH model (panel b, GFDL winds) and the WNA model (panel c, GFS winds). From top to bottom, the wind fields are valid for 0730 UTC September 13, 1330 UTC September 15, 1030 UTC September 17, and 1030 UTC September 18, respectively.

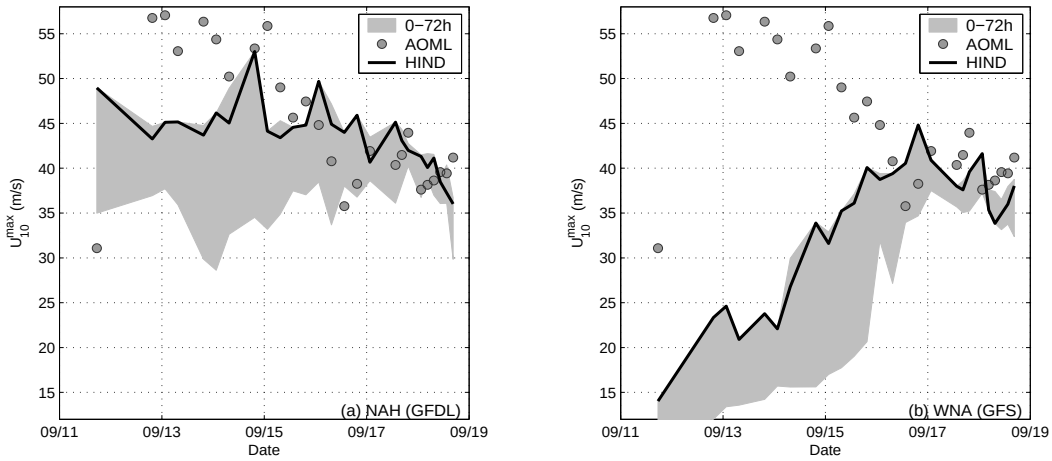

Fig. 3.2 : Maximum wind speeds from the NAH (GFDL) model (panel a) and the WNA (GFS) model (panel b) compared to maximum wind speeds from the AOML analyses as a function of forecast range. Solid line: hindcast / analysis. Shaded area: 0-72 h forecast envelope.

GFS severely overestimated the spatial scales of Isabel. This is illustrated in Fig. 3.1 (first set of panels) with wind fields valid for 0730 UTC September 13. In this figure, the model wind fields are interpolated to the AOML analysis time from hourly fields, while the AOML data are reduced to the spatial resolution of the wave model grids. Note that for a brief period on September 11, the GFDL winds were significantly stronger that the AOML winds (Fig. 3.2).

Through September 14, the comparison between the AOML and GFDL wind fields remained similar, with the maximum wind speeds of the GFDL model becoming more accurate (Fig. 3.2). The WNA (GFS) model gradually improves its representation of Isabel's surface wind circulation and intensity. By the 15th, the circulation in the WNA model has become realistic, although the intensity remains somewhat low (Fig. 3.2). The NAH (GFDL) and WNA (GFS) winds are similar at this stage. This is illustrated in Fig. 3.1 (second set of panels) with wind fields valid for 1330 UTC September 15. At this time Isabel started to reduce in strength as described above, and as is illustrated in Fig. 3.2.

From this time on, Isabel began to grow in size while losing some intensity. The NAH (GFDL) wind speeds intensities were realistic, but the spatial extent of its wind fields is generally smaller than in the AOML analysis. In this period, the WNA (GFS) wind fields showed a better representation of the size of Isabel. However, GFS intensities were somewhat low, and maximum wind speeds of the GFS model were systematically lower than the maximum wind speeds of the GFDL model. In general both model wind fields compare well with the AOML data, as shown in Fig. 3.1 (bottom sets of panels) and in Fig. 3.2 for 0130 UTC September 17, and 1030 UTC, September 18.

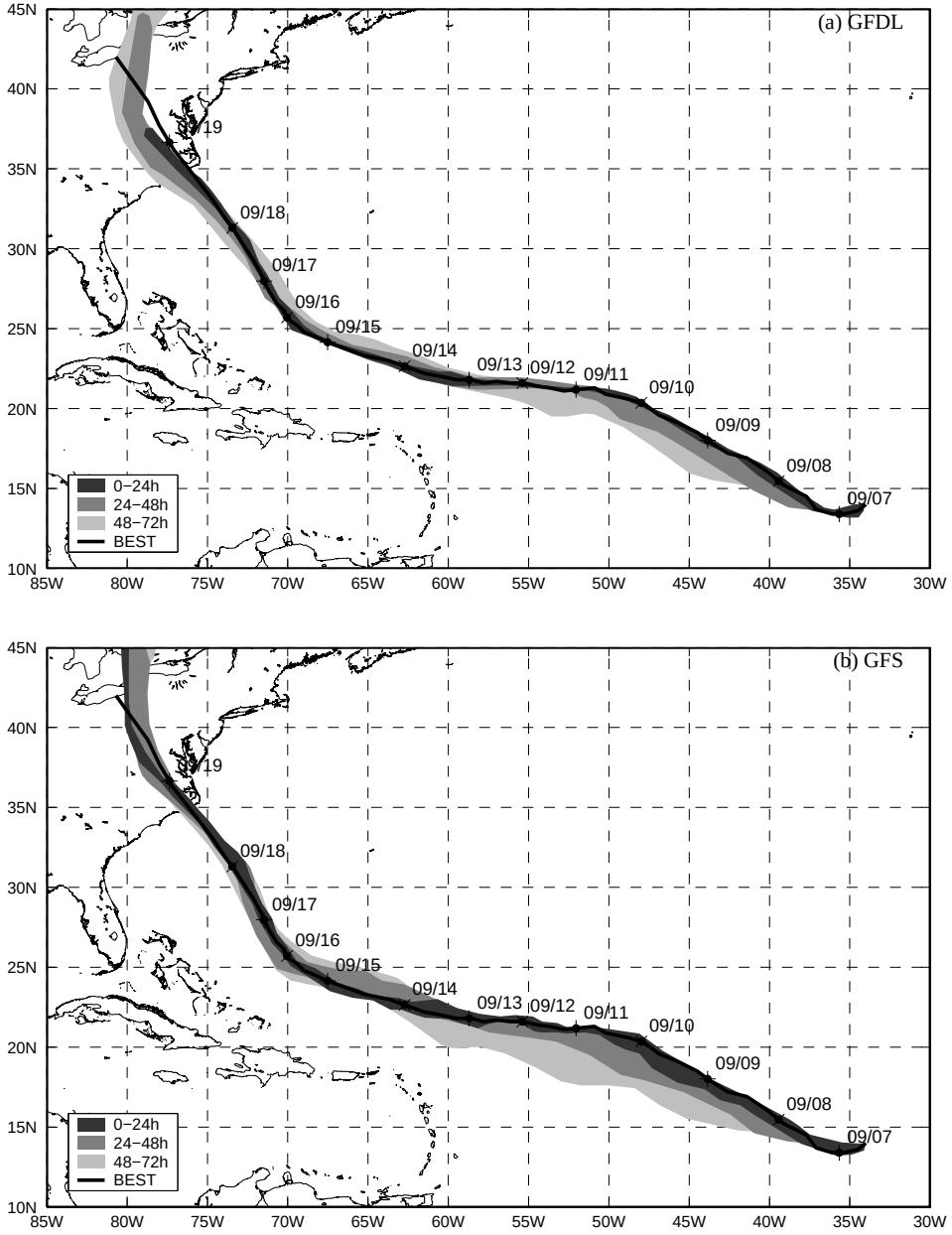

Fig. 3.3 : Track forecasts for Isabel from the GFS (WNA) model (panel a) and the GFDL (NAH) model (panel b). Shading identifies tracks for various forecast ranges. Best track from TPC advisories.

So far, we have assessed only the wind fields used in the hindcast of the wave models. When forecast winds are considered, one critical aspect of the hurricane forecast other than the wind intensity is the track forecast. Figure 3.3 identifies track forecast ranges for the GFS and GFDL models as used in the WNA and NAH wave models, respectively. Both models accurately capture the track of Isabel up to the 72 h forecasts, which is the forecast horizon for the NAH model. Generally, the GFDL model (Fig. 3.3b) shows a narrower envelope of tracks around the analyzed track, and hence produces better track forecasts than the GFS model (Fig. 3.3a). Near landfall, however, the GFDL model predicted a track that is systematically to the left of the analyzed track, whereas in this time frame, the GFS model produced a narrower and less biased envelope of tracks.

The quality of the wind intensity forecasts is assessed in Fig. 3.2 with forecast envelopes of maximum wind speeds. For both the NAH and WNA (GFS and GFDL) wind fields, forecast maximum wind speeds were systematically lower than the hindcast (analysis) maximum winds. For both models, the underestimation appears the largest when Isabel was most intense and relatively small. Near landfall, when Isabel is less intense and much larger, the forecast wind speeds remained much closer to the analyzed wind speeds. Thus, forecasts are expected to be of good quality near landfall, but less so in the early stages of Isabel's life.

For wave model forecasts, the final critical aspect of the hurricane wind field forecast is the timing. The timing of Isabel in the GFS and GFDL models will be addressed in the following section through the analysis of wave height forecast envelopes at selected buoy locations.

This page is intentionally left blank.

4 Wave height prediction

The validation of the wave models will first concentrate on the prediction of the significant wave height H_s. Instead of adding measures for the wave period to this initial assessment, a more complete spectral analysis will be presented in a separate section below. As with the wind fields, we will first concentrate on the model hindcasts of H_s. We will then analyze the quality of the forecasts, using envelopes of forecasts up to 72h.

For most of its life cycle Isabel was far from the buoy observation network off the eastern US coast. Thus, buoy data provides a good record of the extreme wave conditions only when Isabel approached land. The availability of altimeter measurements of H_s from Jason-1 allows us to extend our analysis to areas far from the coast. Several "direct hits" of altimeter tracks on the core of Isabel were found. This allows us to address model accuracy with respect to extreme wave conditions throughout the life cycle of Isabel in both deep water and near the coast.

Model validation with altimeter data will be considered first, concentrating on hindcasts. Buoy data will be used subsequently to assess the quality of the model results, for both wave model hindcasts and forecasts.

4.1 Hindcast validation using Jason-1 data

Four altimeter passes through Isabel have been identified as direct hits. For these four passes, wave height fields from the WNA and NAH models, as well as model data collocated with the altimeter track are presented in Fig. 4.1. The Jason-1 data are presented at native resolution (without averaging or smoothing). Model wave fields are interpolated from hourly outputs into the mean time of the altimeter track positions, while the collocated model data are obtained by tri-linear interpolation of hourly wave height fields into individual track positions and times.

The first two tracks presented in Fig. 4.1 represent the early and most intense stages of Isabel's life cycle. As discussed in the previous section, the GFS winds do not yet capture Isabel adequately. Consequently, the WNA model severely underestimates the wave heights. The NAH model produces much more realistic wave heights, but appears to have a tendency to overestimate the maximum wave heights. The first track (Fig. 4.1a), however, corresponds to a period where the AOML wind analysis suggests that the NAH winds are too strong (Fig. 3.2). As could be expected, the NAH model overestimates the Jason-1 data along this entire track. For the second track (Fig. 4.1b), the NAH model uses significantly lower winds than analyzed by AOML (Fig. 3.2). Wave heights nevertheless appear to be well predicted by the NAH model. Note that in the area where maximum wave heights are expected according to the NAH model results, altimeter data

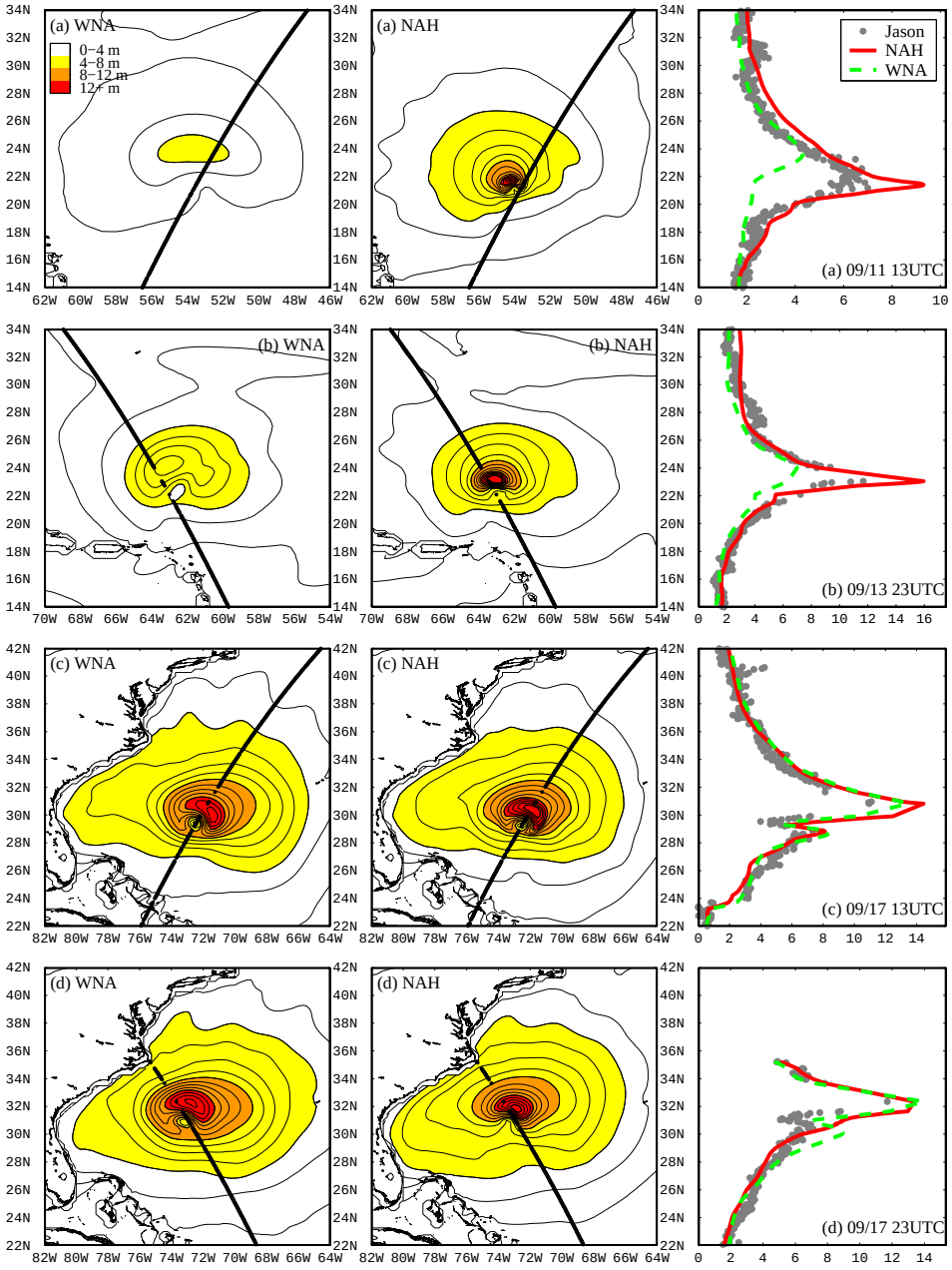

Fig. 4.1 : Wave heights H_s in meters from the WNA model (left panels) the NAH model (center panels) and corresponding model data collocated with Jason-1 altimeter data (right panels) for tracks cutting through Isabel. Model fields from closest hindcast hour. Model and altimeter data collocated by interpolation in space and time from hourly wave height fields. (a) 9/11 1300 UTC fields. (b) 9/13 2300 UTC fields. (c) 9/17 1300 UTC fields. (d) 9/17 2300 UTC fields.

shows large drop out rates. This hampers a proper assessment of the maximum wave heights for the tracks presented in Fig. 4.1b through d.

For the two tracks presented in Fig. 4.1c and d, Isabel is near landfall, has decreased in intensity, but increased in size. At this stage, GFS and GFDL wind fields are similar and of good quality, as discussed in the previous section. Consequently, the WNA and NAH wave models produce similar wave fields, closely reproducing the Jason-1 observations. Two details of these figures deserve additional attention. First, on the 17th 1300 UTC, the altimeter track passes very close to the eye of Isabel, resulting in a very sharp dip in observed wave heights near the eye. This dip is reproduced with high accuracy by both wave models, in spite of the fact that the resolution of the wave model (25 km) is significantly poorer than the along-track resolution of the altimeter (7 km). Second, on the 17th 2300 UTC south of Isabel, the NAH model results in more accurate predictions, yet the WNA model more accurately describes the spatial wave height pattern with lower wave heights near the eye of Isabel.

Data from four selected tracks sampling swell fields generated by Isabel are presented in Fig. 4.2. The first two sets of data (the 14th 1400 UTC and the 15th 0000 UTC) represent swell fields ahead of the hurricane. For both tracks the swells generated by the NAH model are significantly larger and in better agreement with observations than the swells generated by the WNA model. This can be explained by the fact that the winds in the WNA model severely under predicted Isabel over the preceding days. When Isabel approaches land, the differences between the NAH and WNA models become smaller, as will be illustrated with the buoy data below.

The last two panels in Fig. 4.2 represent tracks that captured swell fields behind Isabel. For the data for the 11th 2300 UTC, the differences are similar to the model differences for tracks ahead of Isabel, and differences between the models are most likely due to the underestimation of Isabel in the GFS model. For the 19th 1200 UTC the pattern is reversed. To the right of Isabel, and behind Isabel, the WNA model overestimates swell wave heights, whereas the NAH model shows lower but still more realistic swells. At this stage Isabel has made landfall, but the differences in model results can only be due to the different GFS and blended GFDL/GFS wind fields used to represent the hurricane previously. Note furthermore that this appears to be a systematic pattern that can be observed in several Jason-1 passes starting on the 16th.

Two additional observations can be made from Fig. 4.2. First, the altimeter data show distinctive spatial variability on small scales. This suggests that the typical "pulsating" nature of hurricane wind fields indeed results in the generation of many individual swell fields. This complicates prediction and validation of swells generated by hurricane wave models. Second, the wave model seems to show some variability of H_s at similar spatial scales. However, practical experience indicates that this is an artifact of discretization of the spectral space in

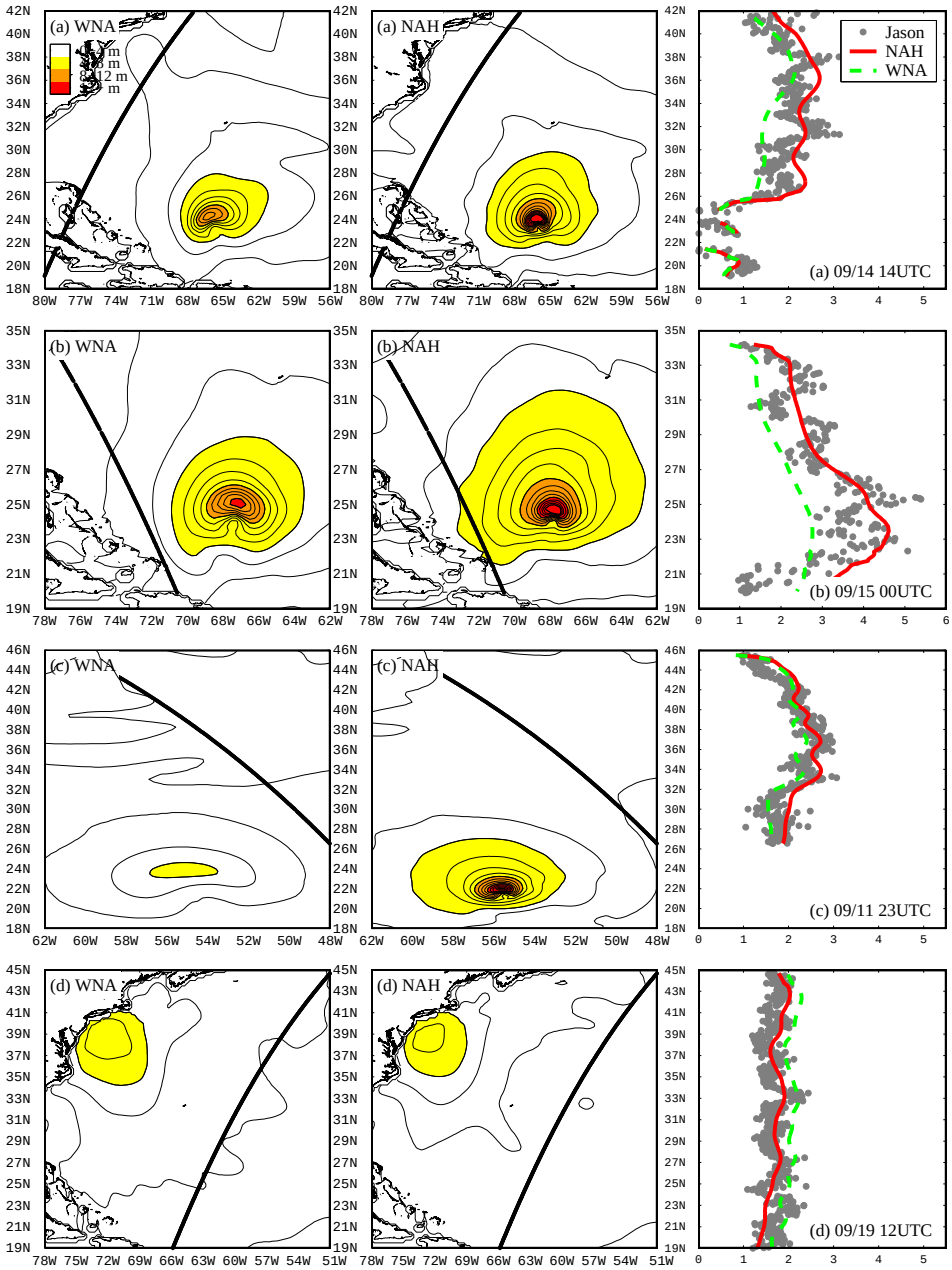

Fig. 4.2 : Like Fig. 4.1 for selected Jason-1 tracks with dominant swells from Isabel. (a) 9/14 1400 UTC fields. (b) 9/15 0000 UTC fields. (c) 9/11 2300 UTC fields. (d) 9/19 1200 UTC fields.

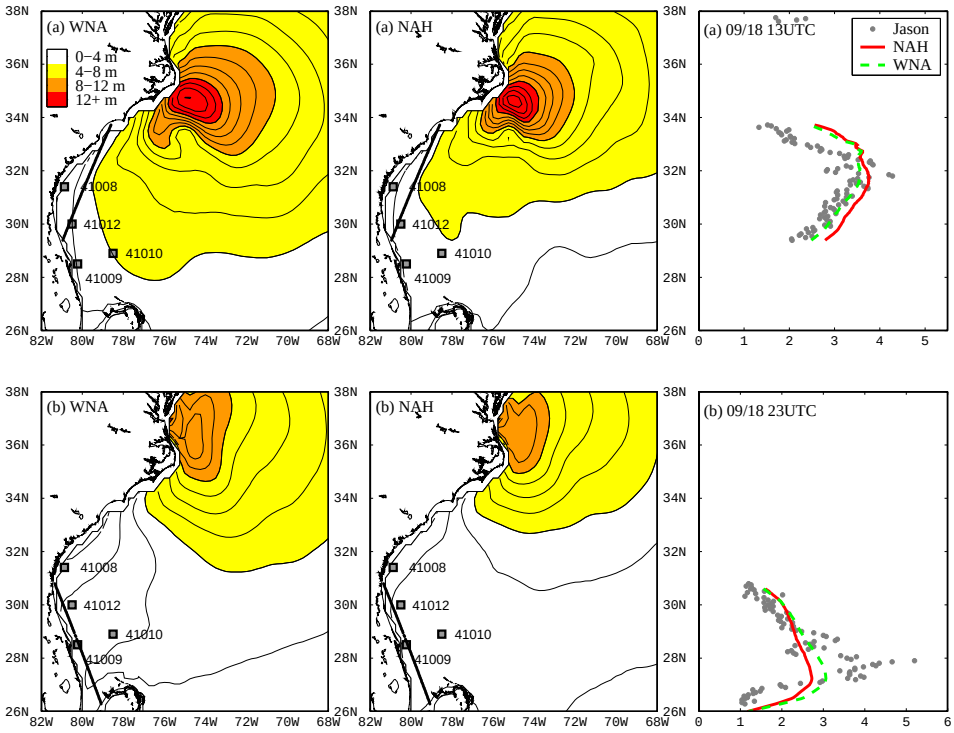

Fig. 4.3 : Like Fig. 4.1 for selected Jason-1 tracks near the southern US coast near landfall of Isabel. (a) 9/18 1300 UTC fields. (b) 9/18 2300 UTC fields.

numerical wave prediction models (Booij and Holthuijsen, 1987; Tolman, 2002b), and not due to the physics of the processes expected to be responsible for the variability in the observed wave heights.

Finally, two Jason-1 tracks provide observations along the coast for the southern United States. Data for these tracks are presented in Fig. 4.3. For both tracks, the models show reasonably good results, but also some deficiencies. First, both models systematically over predict wave heights for both tracks close to the coast. Second, wave heights are severely under predicted by both models in the Gulf Stream region (between 27 and 28°N in Fig. 4.3b). Both aspects of the model will be discussed in more detail below.

4.2 Hindcast validation using buoy data

Wave measurements are available for the 15 NDBC buoys identified in Fig. 2.1. Time series of the significant wave height H_s from the hindcasts of both wave models are presented in Figs. 4.4 through 4.7. The buoys are grouped in the figures by geographical region. The time series present data from the 12th 0000 UTC through the 22th 0000 UTC, representing the period in which wave conditions at buoy locations were influenced by Isabel.

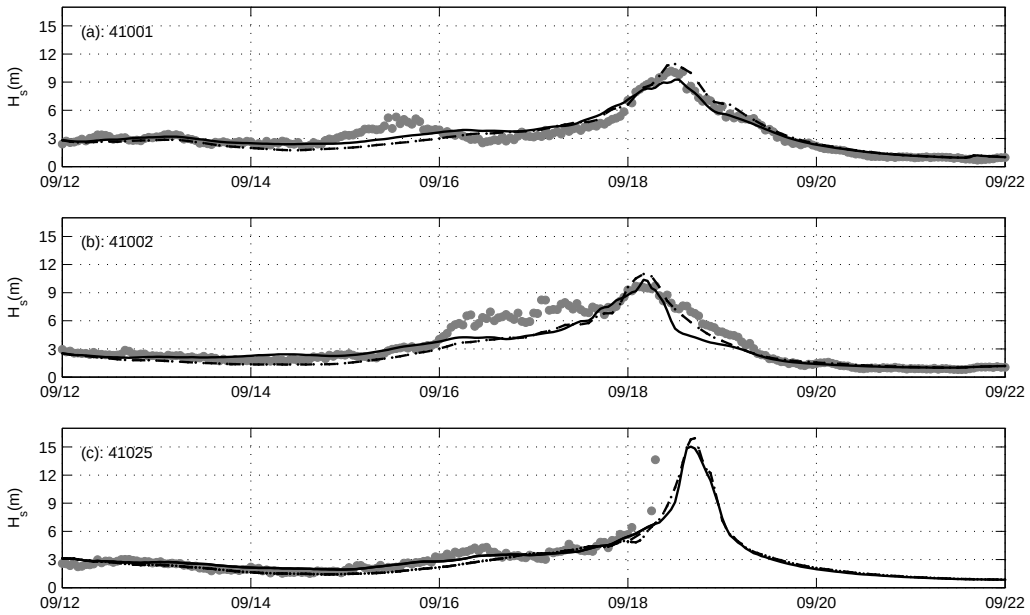

Fig. 4.4 : Hindcast wave heights H_s from the WNA model (chain line line), the NAH model (solid line) and the buoy observations (•) for the buoys nearest to Isabel's track (a) 41025, (b) 41002, and (c) 41001.

The most extreme wave heights are concentrated fairly close to the track of Isabel, with maximum wave heights from 10 to 15 m for the buoys in Fig. 4.4. Away from the track, wave heights rapidly decrease but are dominated by waves from Isabel at all buoys. Maximum wave heights at the southern and northern most buoys (41009, Fig. 4.5d and 44011, Fig. 4.7b) reach 4 m. This implies that the 12 ft wave height threshold as used by TPC in their advisories was in essence reached for the entire US Atlantic seaboard. This threshold was not reached at only two buoys; buoy 41008 (Fig. 4.5d), which is in shallow water, and buoy 44005 (Fig. 4.7d), which was somewhat sheltered in the Gulf of Maine.

Buoy 41025 was rendered inoperable by Isabel, as mentioned in Section 1. The last observation at this buoy appears anomalously high. For the last two observations at buoy 41025, the wave height $H_s \geq 0.5d$, where d is the mean water depth. This implies that buoy was in surf zone conditions, with vigorous depth-induced breaking of many waves. This eventually resulted in the buoy breaking off its mooring. If the mooring had already separated during the last 20 min period for which a wave height observations are available, massive horizontal accelerations due to breaking waves are likely to have been interpreted as vertical accelerations, resulting in a spuriously height wave height observation. The last wave height observation at this buoy is therefore suspect.

From the 12th through the 17th, the NAH wave model produced higher wave heights than the WNA model for all buoys. This can be attributed to the fact

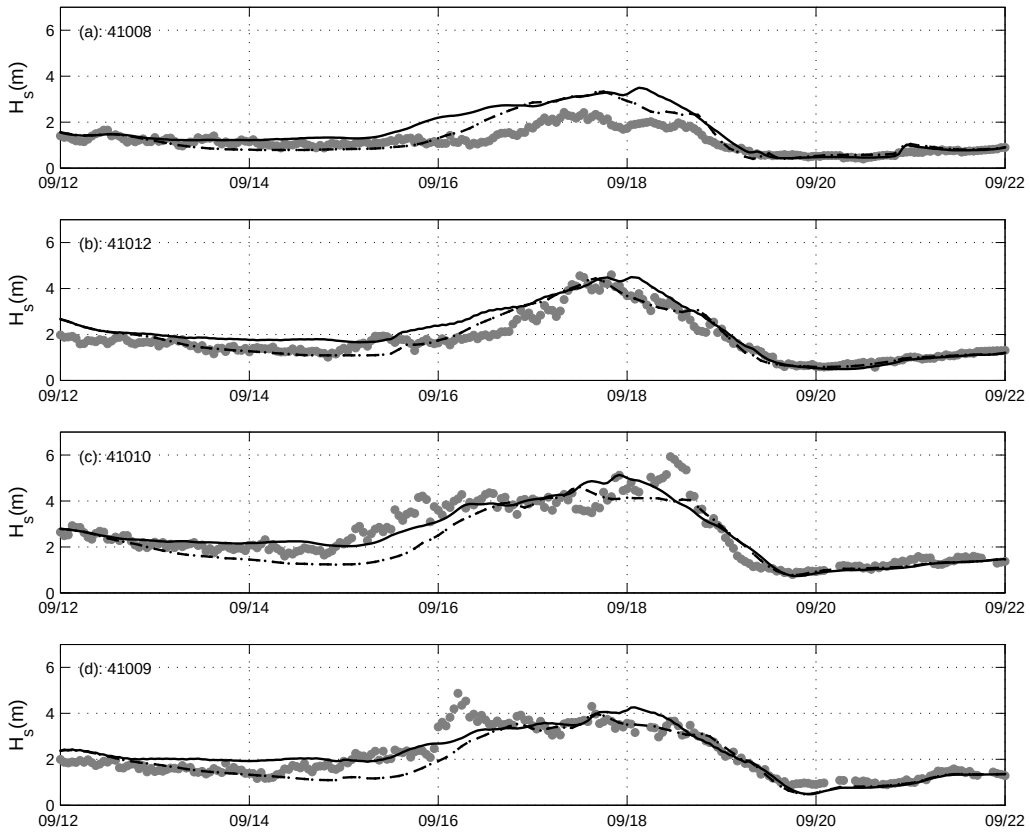

Fig. 4.5 : Like Fig. 4.4 for buoys south of Isabel's track. (a) 41008, (b) 41012, (c) 41010 and (d) 41009.

that wind speeds in the GFDL (NAH) model were systematically higher than in the GFS (WNA) model through the 15th, while Isabel was a category 4 or 5 hurricane far from the coast. The corresponding swells reached all buoys in this period, as will be shown in the following section. From the 17th on, wave heights of both models are very similar, with typically wave heights from the WNA model marginally higher. This can attributed to the fact that the spatial scales of the wind fields in the GFS (WNA) model are systematically larger than in the GFDL (NAH) model. The larger size of Isabel in the GFS model apparently makes up for the slightly lower wind speeds (when compared to the GFDL winds).

Both wave models generally give a good description of the most extreme wave conditions generated by Isabel, which occur from the 17th through 19th, depending on the actual buoy locations. Two model deficiencies can be observed in the validation against buoy data. First, a wave event can be identified on the 15th and/or the 16th that appears to be missed by both models. This is particularly clear for buoys 41001, 41002, 41009 and 44004 (Figs. 4.4c, 4.4b, 4.5b, 4.6d, respectively), but can be observed at virtually every buoy. As will be shown in Section 5, this can be attributed to the underestimation of Isabel's

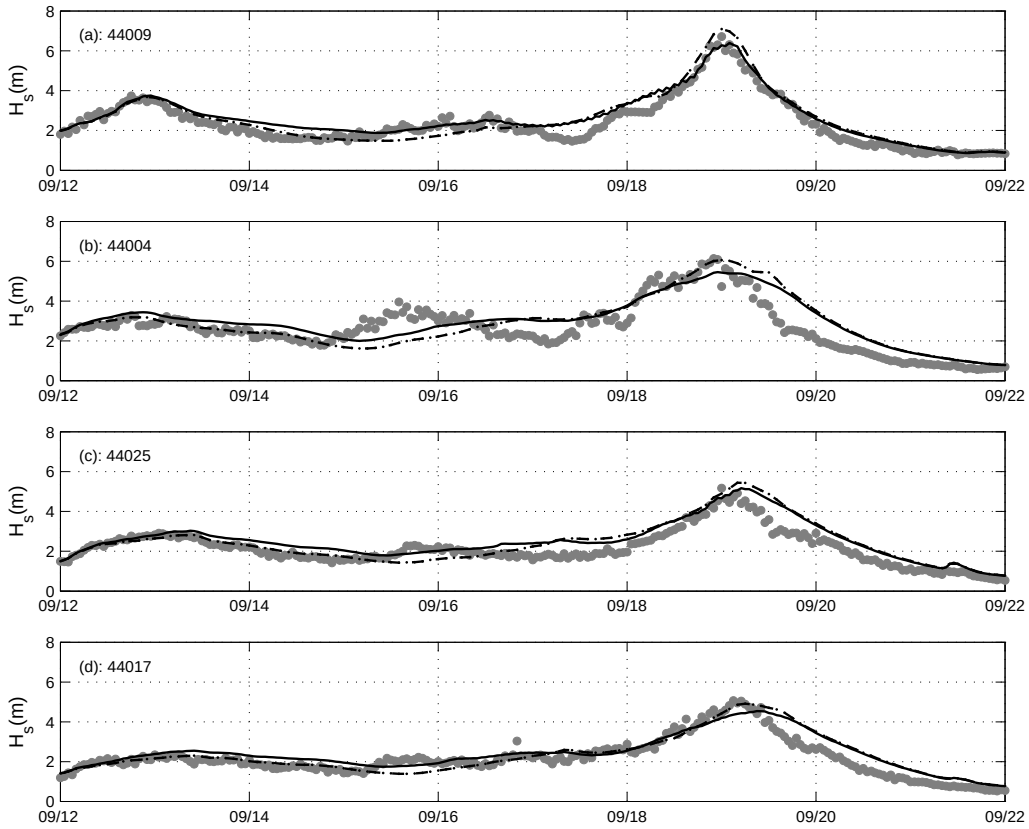

Fig. 4.6 : Like Fig. 4.4 for buoys north of Isabel's track up to Long Island. (a) 44009, (b) 44004, (c) 44025 and (d) 44017.

wind speed in both models, while Isabel was at maximum strength. Second, both models significantly overestimate the wave heights at buoy 41008. This is consistent with the Jason-1 altimeter data in Fig. 4.3, and appears to be due to inadequate modeling of shallow water effects in the shelf regions. This will be discussed in more detail in Section 6.

Several buoys show what appears to be a diurnal cycle in the measured wave heights. This is particularly clear at buoy 41018 (Fig. 4.7c). This suggests an interaction between the wind waves and the local tides. The latter buoy also shows a small but persistent oscillation with a period of 2 h (or twice the model time step) for the NAH model. These aspects of the model results will also be discussed in more detail in Section 6.

Figures 4.4 through 4.7 indicate qualitatively that both wave models have the potential of providing accurate guidance for forecasting. Quantitative measures for the wave model hindcasts are presented in Table 4.1 for all buoys. Presented are conventional metrics used in wave modeling: the model bias, the rms wave height error and the scatter index (S.I.) defined here as the rms errors normalized with the mean observed wave heights. All these metrics have been calculated for

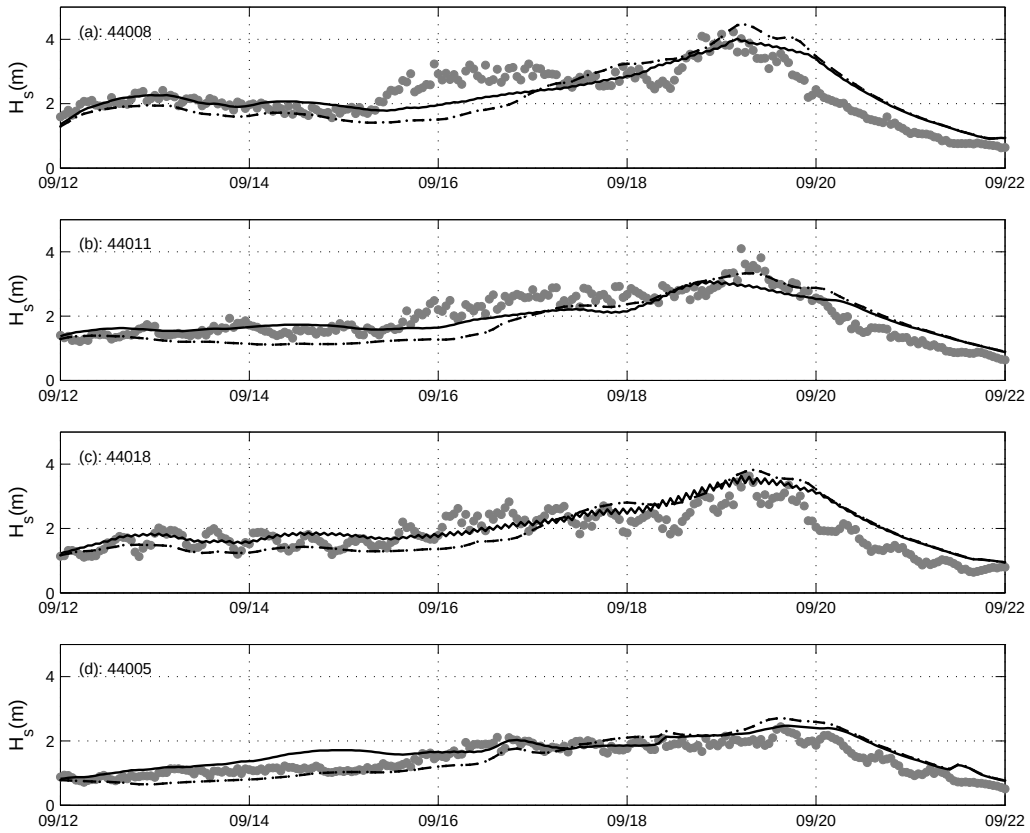

Fig. 4.7 : Like Fig. 4.4 for buoys far north of Isabel's track. (a) 44008, (b) 44011, (c) 44018 and (d) 44005.

the 10 day period for which time series are shown in Figs. 4.4 through 4.7. With few exception, biases of both models are small. The SI and rms errors are larger than for typical model validations over long periods, but fairly typical for event analyses. For the most part, the NAH model clearly outperforms the WNA model in terms of rms errors and SI. The exceptions are buoys 41008 and 41012, where the WNA model severely overestimates the wave heights on the shelf, and where the positive bias is increased in the NAH model due to the added swells from Isabel.

Table 4.1: Bulk statistics of model hindcasts for all buoy locations.

		NAH model			WNA model		
buoy	depth	bias	rms	S.I.	bias	rms	S.I.
	(m)	(m)	(m)	(%)	(m)	(m)	(%)
41025	18.9	-0.01	0.68	23	-0.35	0.80	27
41001	4,389	0.02	0.62	18	-0.05	0.79	23
41002	3,786	-0.40	1.04	30	-0.57	1.02	29
41008	18.0	0.42	0.64	55	0.19	0.48	42
41012	38.4	0.30	0.47	26	0.06	0.34	19
41010	841.2	-0.03	0.48	18	-0.34	0.68	26
41009	42.0	0.07	0.44	20	-0.21	0.52	24
44009	28.0	0.26	0.38	16	0.18	0.41	17
44004	3,164	0.30	0.69	26	0.21	0.78	29
44025	40.0	0.38	0.50	23	0.30	0.54	25
44017	52.4	0.24	0.43	20	0.14	0.44	20
44008	62.5	0.05	0.48	21	-0.04	0.64	28
44011	88.4	-0.04	0.37	18	-0.15	0.46	23
44018	56.7	0.21	0.42	23	0.10	0.55	29
44005	21.9	0.23	0.31	22	0.03	0.34	24

4.3 The quality of the forecasts

So far, we have only considered model hindcasts of significant wave heights. For a forecaster, these only present the potential accuracy of their guidance. The accuracy of the model forecasts can concisely be addressed using envelope plots as used for wind fields in Section 3. Figure 4.8 presents such envelopes for 72 h forecasts from the NAH model. Also shown in this figure are the confidence limits for the buoy observations. Buoy observations are known to include a significant sampling uncertainty, due to the brevity of the time series used and the stochastic nature of wind waves (e.g., Donelan and Pierson, 1983). The corresponding 95% confidence limits of the buoy data, calculated according to Young (1986), are represented in Fig. 4.8 by two sets of solid lines. The first three buoys for which data are presented in this figure (41001, 41002 and 44009) are selected for their proximity to the track of Isabel. Wave heights at these locations are expected to be most sensitive to forecast errors in the track of Isabel. The other three buoys (41010, 44008 and 44018) were selected as representative for different areas along the coast. Results for the WNA model show similar envelope behavior, and are not presented here.

The envelopes of forecast wave height are very narrow, and the range of wave heights in the envelope is comparable to the range of wave heights defining the

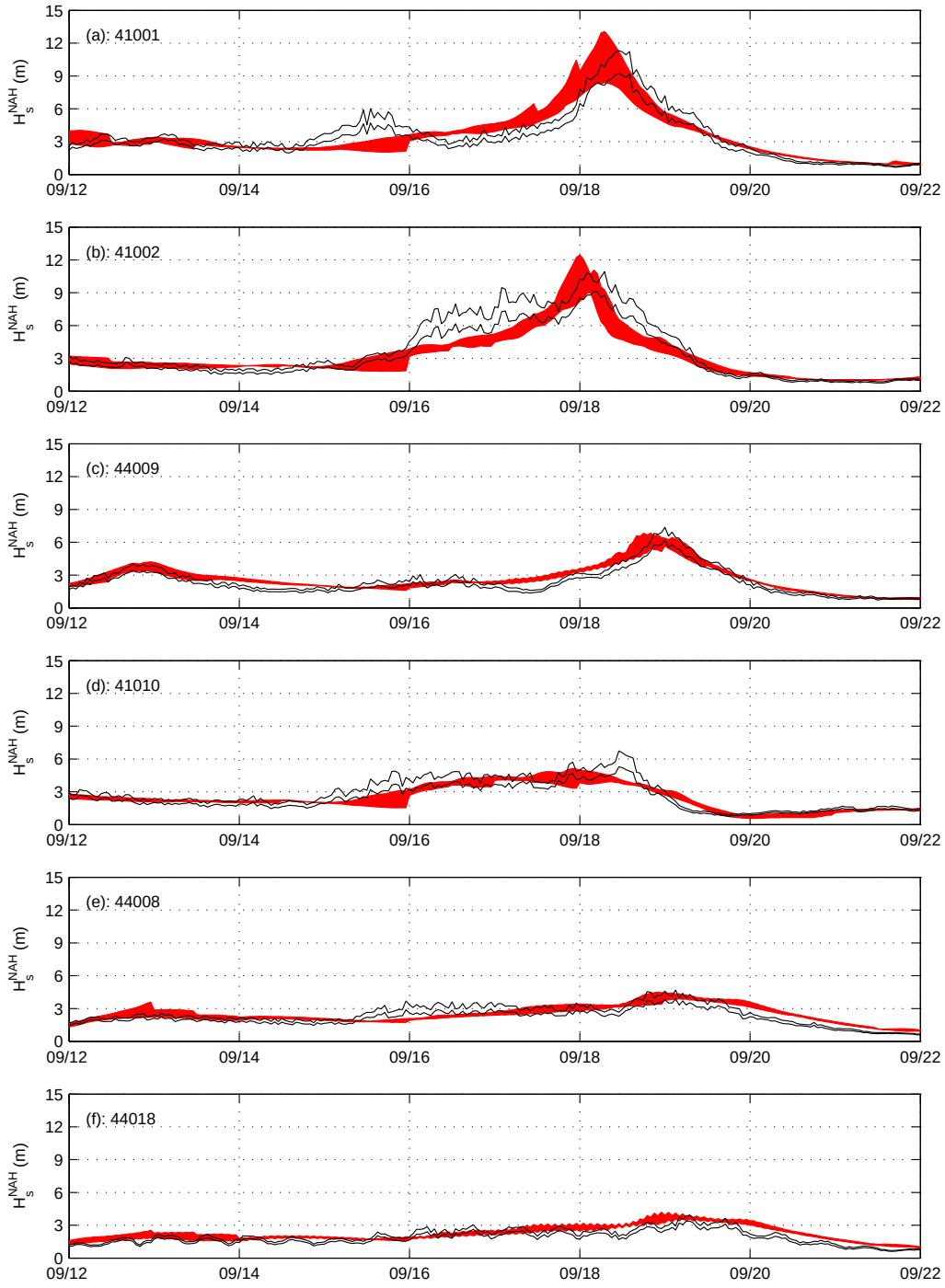

Fig. 4.8 : Envelope of wave heights H_s for 0 to 72 h forecasts (gray shading) of the NAH model and 95% confidence limits of observed wave heights (thin solid lines) for buoys (a) 41001, (b) 41002, (c) 44009, (d) 41010, (e) 44008, and (f) 41018.

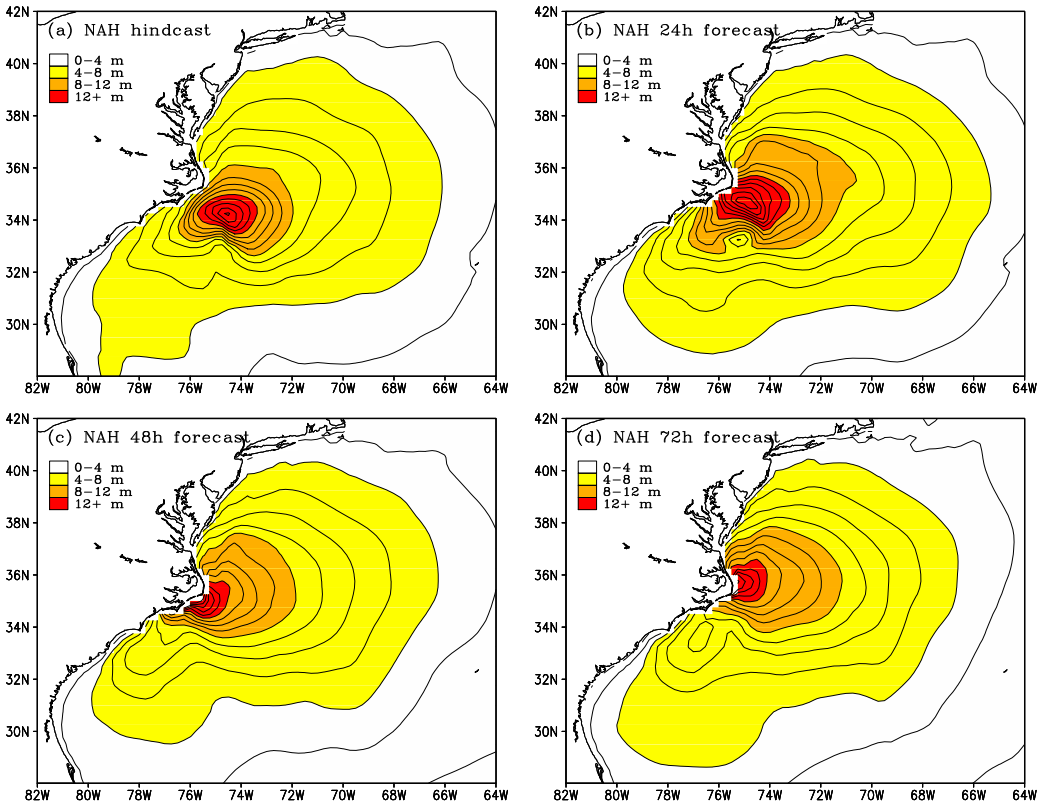

Fig. 4.9 : Wave height fields from NAH model valid for 9/18 1200 UTC from (a) hindcast, (b) 24 h forecast, (c) 48 h forecast, and (d) 72 h forecast. Contours at 1 m intervals, shading as in legend.

confidence limits of the observations. For swells far away from the track this might be expected, as many swell fields in the forecast are in fact generated by analyzed rather than forecasted wind fields. It is somewhat surprising to see that the envelopes are also very narrow for the extreme wave conditions near the track. This indicates that the wind forecasts for both the GFS and GFDL model near landfall were excellent, which translated into excellent wave forecast up to the 72 h forecast horizon.

Another way of assessing the usefulness of forecasts is to compare wave height fields for a given valid time from several model cycles. Due to the potential of damage to life and property, a time period close to landfall is most interesting. Figure 4.9 shows wave height fields near landfall on the 18th 1200 UTC from the NAH model for the hindcast, and the corresponding 24, 48 and 72 h forecasts. In the hindcast (Fig. 4.9a), the maximum wave height is just over 16 m, and severe conditions with wave heights $H_s > 12$ m are concentrated in a well defined area just offshore off Cape Hatteras. The $H_s = 4$ m contour, which is near the 12 ft threshold level used in the advisories of TPC, covers a large area. The extent of

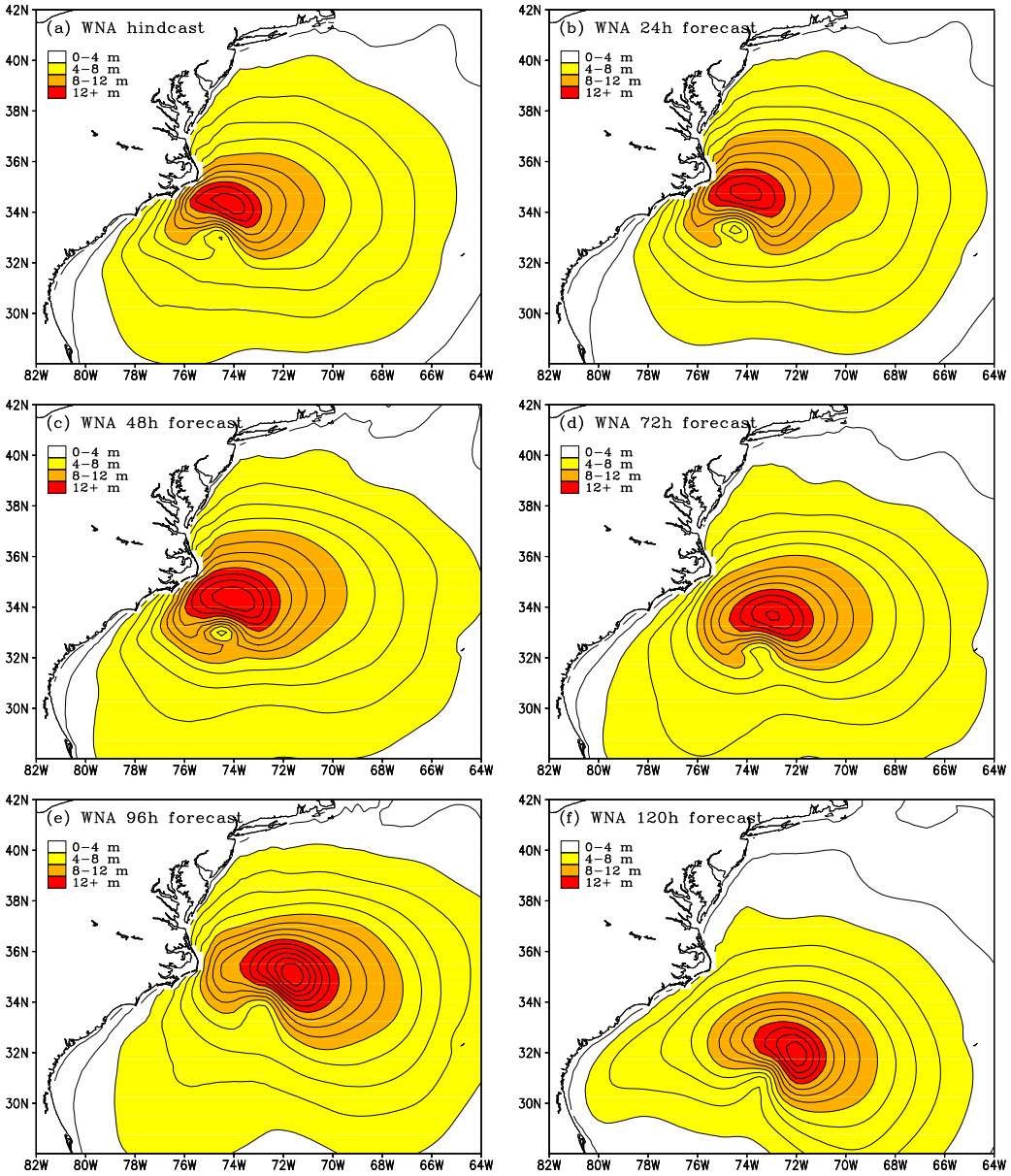

Fig. 4.10 : Like Fig. 4.9 for WNA model, adding (e) 96 h and (f) 120 h forecast.

this contour from the center of Isabel varies enormously per quadrant, as noted in the advisories of TPC. The three forecasts valid for this time show similar height distributions and maximum wave heights, with the latter reaching the coastline around Cape Hatteras. The major difference is that the (GFDL) forecasts take Isabel on shore somewhat too quick. Figure 4.9 nevertheless clearly shows the value of the wave forecasts of the NAH model up to its forecast horizon of 72 h.

Figure 4.10 shows similar results from the WNA model. Qualitatively these are similar to the results of the NAH model, with the (GFS) forecasts taking Isabel to the shore at a slower pace. The WNA model forecast horizon is 7 days, and 4 and 5 day forecasts from the WNA model are also presented in Fig. 4.10e and f. For these forecasts, track and timing errors grow larger, as would be expected, but the structure, intensity and general direction of Isabel's wave fields are captured well. Note that the maximum wave heights in both Figures consistently range from 15 to 18 m, consistent with the narrow envelopes of forecast wave heights at buoy locations in Fig. 4.8.

5 Evolution of spectra

So far, the assessment of the operational wave model behavior has only been made by considering the overall significant wave height H_s. However, much more information is available from buoy observations through the one dimensional spectrum of wave energy $F(f)$, where f is the spectral frequency. In some cases the buoys even provide directional information, allowing estimates of the two dimensional spectra $F(f, \theta)$, where θ represents the spectral direction (in the present area and time of interest, only buoy 44025). The latter spectrum is the fundamental predicted product of the wave model, and is produced as output for all buoy locations by the WNA and NAH models[8]. The two-dimensional model spectrum $F(f, \theta)$ is reduced to the one-dimensional spectrum $F(f)$ by integration over the direction θ.

Many validation studies extract the peak period T_p from the model and the observations for validation purposes. However, due to the discontinuous nature of T_p, such a comparison can be rather misleading. A presentation of more comprehensive spectral data is therefore justified. Visualization and analysis of such spectral data for studying swell propagation was pioneered by Munk (1947) and Barber and Ursell (1947). In these papers, it is shown that a display of $F(f; t)$, with t representing time, can identify the dispersion characteristics of individual swell systems. Recognizing their pioneering work, we will designate such plots as Munk-Barber-Ursell (MBU) plots. Conciseness does not allow us to present such figures for all buoys. We have therefore selected some buoys to be both representative for areas, as well as for their peculiar details. Buoy 41001 is chosen as representative for near the track of Isabel. Buoy 41018 is chosen as representative for the northern buoys. Buoy 41012 is chosen as representative for the southern buoys.

Figures 5.1 through 5.3 show the MBU plots for the three selected buoys. These Figures present the model results at native spectral resolution from hourly model output, without additional smoothing. To reduce sampling noise in the data, buoy observations have been averaged over 3 h intervals. Note that the buoy data and model results do not share their spectral resolution. In the model, a constant increment factor of 1.10 between discrete frequencies is used, whereas the buoy data are either provided with a resolution of 0.01 Hz throughout spectral frequency space, or with a resolution of 0.01 Hz for frequencies above 0.1 Hz and 0.005 Hz for frequencies below 0.1 Hz. For the present study, only buoys 41008, 41009, 41012, 44017 and 44018 have the higher resolution at low frequencies.

As mentioned above buoy data have a limited accuracy due to the relatively short observation time (20 min per observation), which leads to sampling errors. This is particularly true for the longer wave components in the spectrum, because the number of waves observed in a fixed time interval becomes smaller with

[8] see http://polar.ncep.noaa.gov/waves/products.html

increasing period (decreasing frequency). This decreases the signal to noise ratio with decrease of frequency and hence limits the capability of the buoys to observe small amplitude swells at low frequencies, because they cannot be distinguished from noise (e.g., Earle, 2003). The lowest energy level that can be observed in the buoy data in Figs. 5.1a through 5.3a is therefore limited.

The lowest energy levels at which the wave model can produce swells is limited by the round off errors in the numerical representation of the spectral densities, as well as by possible noise introduced by physical parameterizations. For practical purposes, this energy level is much lower than the lowest energy level than can be observed by buoys. This implies that swell energy can be identified in the model at a much earlier stage of development of an incoming swell field than in the buoy data. For a proper comparison of model results with buoy data it would be appropriate to apply a filter to model data similar to the filter applied to buoy data. However, because this removes much useful information from the model results, we prefer to present model results for the entire resolved energy range in the present figures.

Another eye catching aspect of the MBU plot for the observations at buoy 44018 (Fig. 5.2a) is the apparent diurnal signature, particularly at higher frequencies. This corresponds to a similar cycle in the wave heights in Fig. 4.7c. This appears to be due to wave-current interactions, as will be discussed in the following section.

In the MBU plots, ridges of high energy can be observed. Ridges with a decrease of the local peak frequency with time can generally be identified as growing wind seas. A systematic increase of the local peak frequency can generally be associated with dispersion of swell. If swell is generated at a distance D at a time t_0, the observed frequency f of that swell follows directly from linear wave theory as (e.g., Munk, 1947; Snodgrass et al., 1966)

$$f = \frac{g(t - t_0)}{4\pi D} \quad , \quad \frac{\partial f}{\partial t} = \frac{g}{4\pi D} \quad , \tag{5.1}$$

which implies that pure swell dispersion from a point source results in a ridge in the MBU plot with constant slope $\partial f/\partial t$, and that the intersect of the corresponding line with the time axis at $f = 0$ identifies the time at which the swell field was generated.

A dominant feature for all three buoys considered here is the main signature of the swells as generated by Isabel shortly before landfall, which show clear dispersion patterns (swell ridges) starting early on the 18th at buoy 41001 and late at the 18th at buoys 44018 and 41012. The dispersion pattern shows swell periods dropping from about 15 s to about 6 s in several days (or to about 10 s at buoy 41012). In Figs. 5.1 through 5.3 these dispersion events are identified with the lines marked 'A'. The intersects of the fitted lines with $f = 0$ consistently identify the generation time of these swell fields between 1800 UTC on the 16th

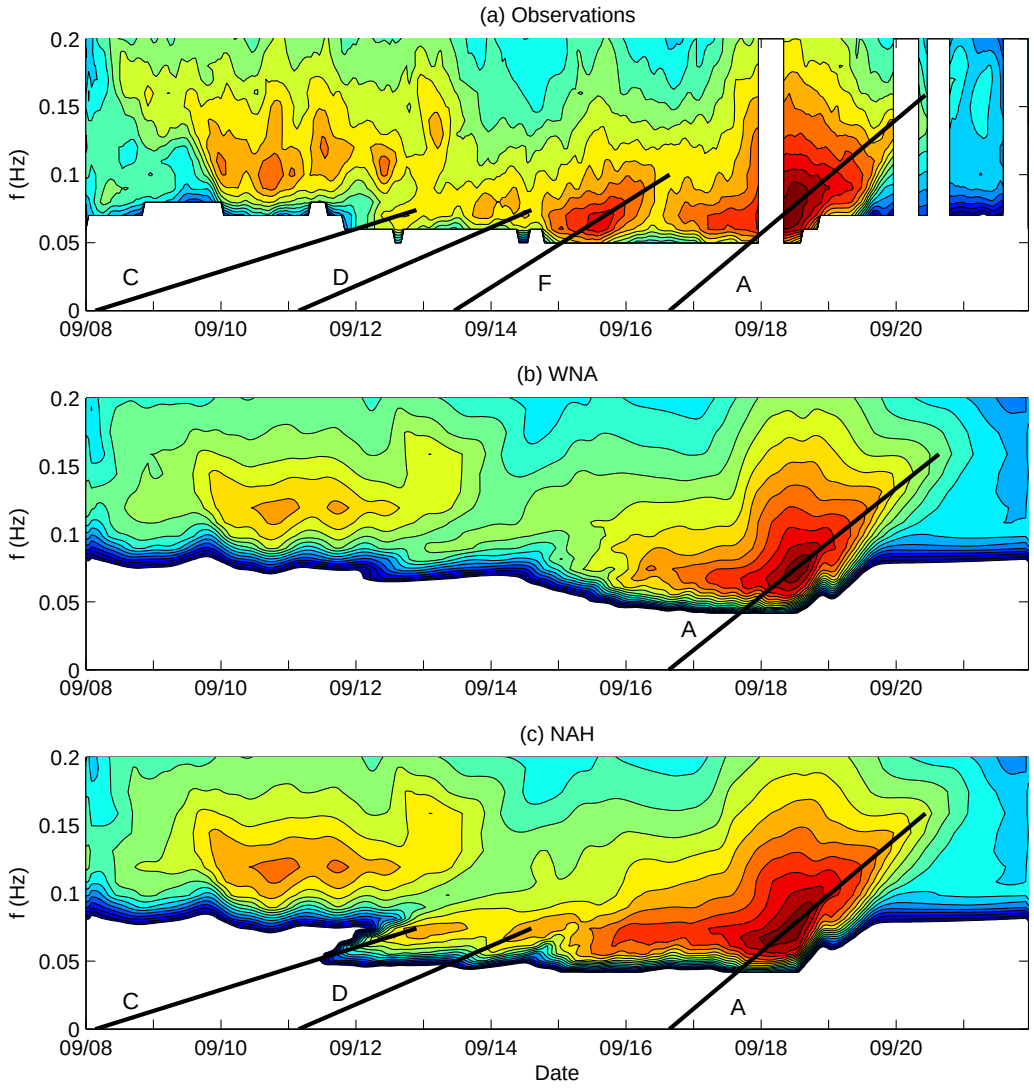

Fig. 5.1 : MBU plot of the wave frequency spectrum $F(f)$ as a function of time t for buoy location 41001. (a) Observations. (b) WNA model. (c) NAH model. Observations averaged over 3 h intervals. Lines A and B are estimated per panel. Lines C through E from NAH model (panel c) and selectively displayed on the buoy data (panel a). Contours from -30 to 30 dB with 2.5 dB increments, and 0 dB corresponding to 10^{-1} m^2Hz^{-1} (as in Snodgrass et al., 1966).

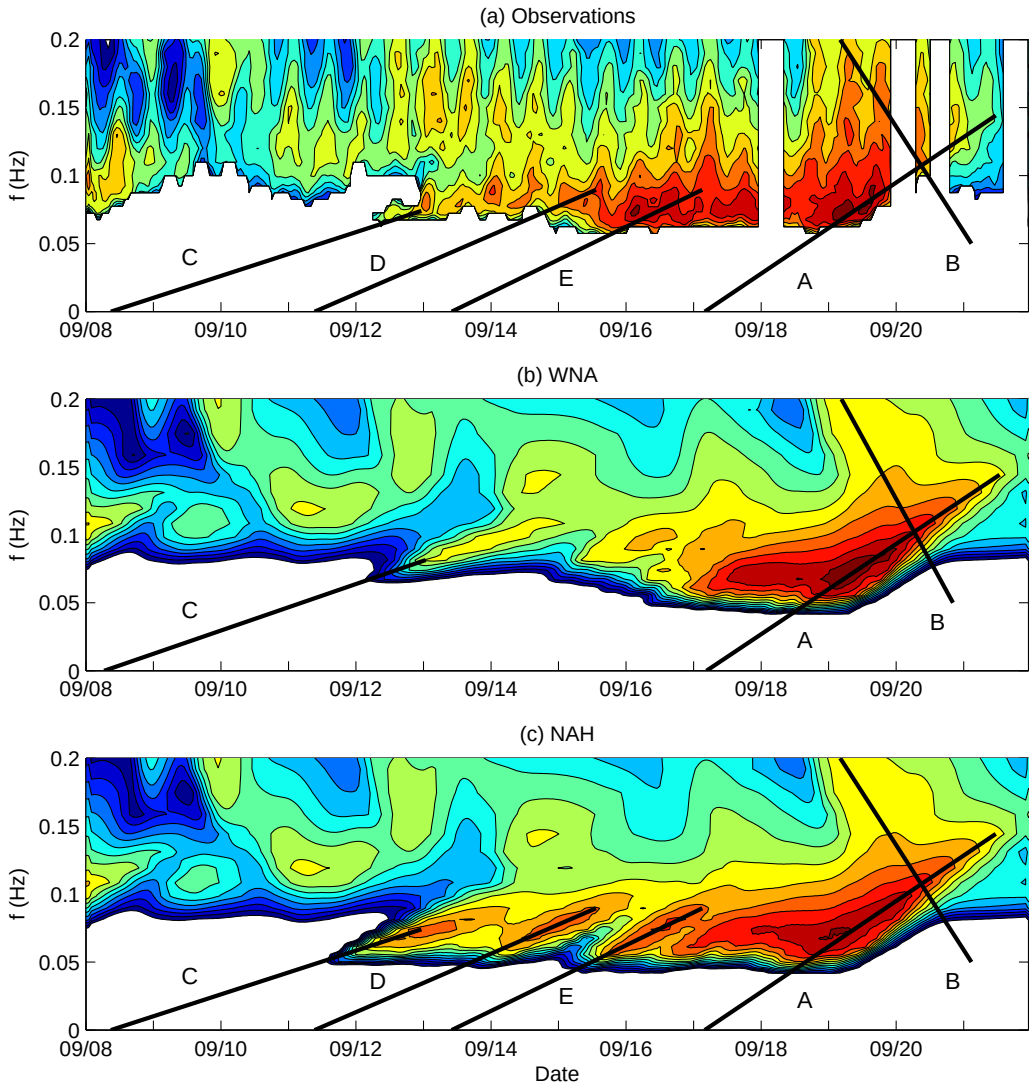

Fig. 5.2 : Like Fig. 5.1 for buoy 44018.

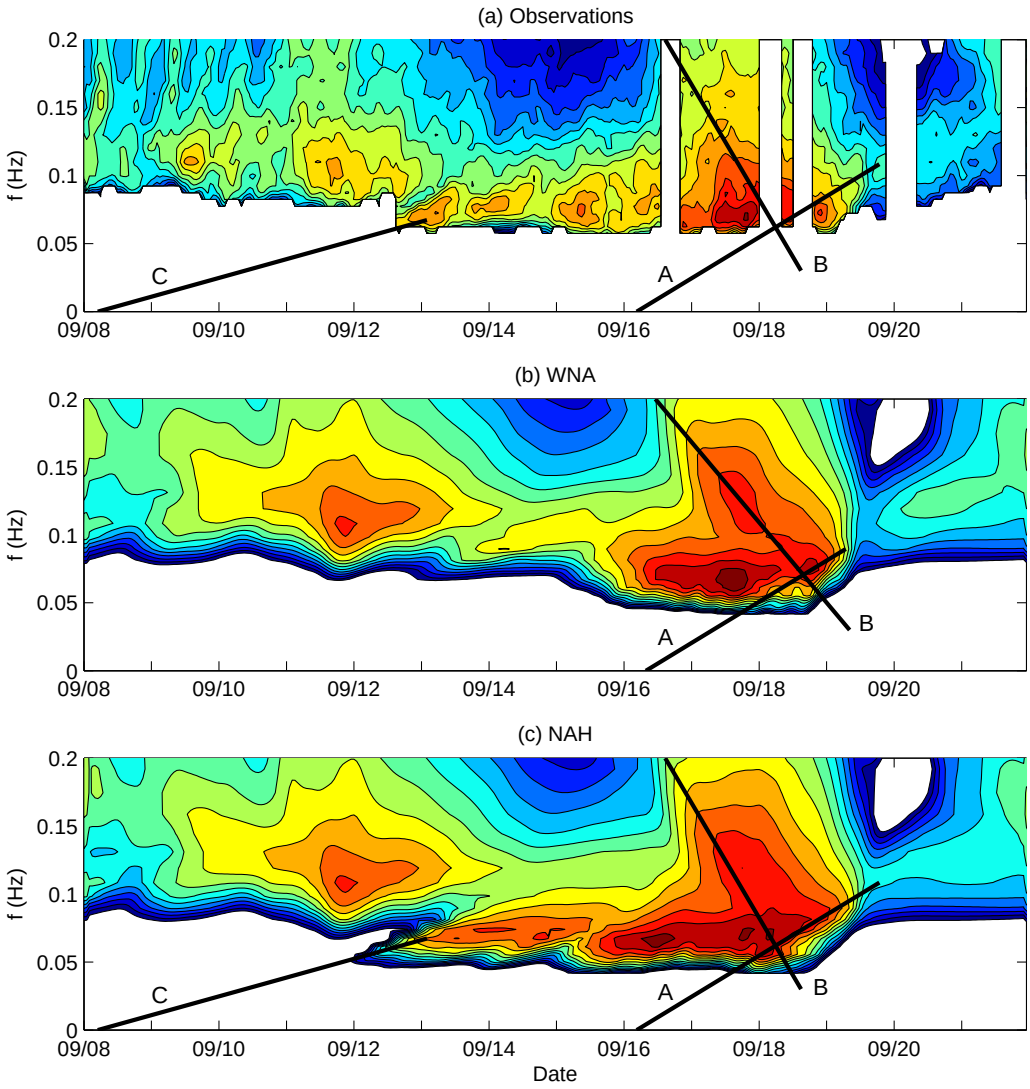

Fig. 5.3 : Like Fig. 5.1 for buoy 41012.

and 0000 UTC the 17th.

Just preceding these events (or coinciding with it) are wave growth events at buoys 44018 and 41012, which are marked with the line 'B' in Figs. 5.2 and 5.3. These events are related to the large scale circulation of Isabel. For buoy 41001 (Fig. 5.1), high energy levels at higher frequencies can also be observed, indicating the presence of a strong wind sea. However, no clear wave growth event can be identified in Fig. 5.1. This is due to a very rapid wave growth, with severe wave conditions in essence arriving simultaneously with Isabel's maximum winds. Note that this is also evident in the buoy data shown in Fig. 4.4.

Before this period, all three buoys recorded persistent swells with a frequency of about 0.07 Hz, which corresponds to a peak wave period of about 14 s, starting on the 12th. These swells lasted up to the 19th when the final swell dispersion pattern starts to evolve. The second part of this period just before landfall is characterized by persistent swells with no discernible dispersion patterns in either observations or model results. For buoy 41001 (Fig. 5.1) this period starts in the NAH model early on the 16th, with the buoy data suggesting that this event started late on the 16th. For buoy 44018 (Fig. 5.2) the second swell period started early on the 17th, and for buoy 41012 (Fig. 5.3) it started around midday the 16th. The lack of dispersion patterns for all buoys in this period indicates that Isabel is sending out swells of similar intensity and period continuously while closing in on land.

The period from the 12th to the 16th is characterized by several features. First, a number of individual swell systems can be identified in the NAH model (c panels of figures). These swell systems are generally absent or severely underestimated in the WNA model (b panels). Because these swell systems were generated when Isabel was a class 5 hurricane, and because GFS (WNA) winds severely underestimated Isabel's winds in this period, the lack of long period swells in the WNA model was expected. Second, the measured data (a panels in figures) show persistent long period (14 s) swells, but without the clear distinction between individual swell systems that can be observed in the NAH model. The lack of structure in the buoy data compared to the model data may be due to two factors discussed above: (i) sampling errors in buoy data and the ambient noise it introduces, or (ii) the lack of resolution in the buoy data for swells due to the signal to noise ratio as discussed above. Considering the above, the discussion of the swell fields from the 12th through the 16th will focus on the NAH model, mainly because of its ability to track swell fields at an early stage.

At all three buoys, the NAH model shows the arrival of the initial swells from Isabel at the buoy locations as represented by the lines marked 'C'. According to the ridge line estimates from the model, these swells originate between 0000 UTC and 1200 UTC on the 8th, which indeed corresponds to the initial stages of Isabel as a hurricane. The ridge lines as estimated from the NAH model (c panels in figures) have been reproduced on the buoy data (a panels in figures) to assess the

quality of the model guidance. Several observations can be made from the ridge lines reproduced on the buoy data. First, the ridge line for the initial swell arrival from the NAH model appears to be mostly related to energy levels that cannot be adequately resolved by in the buoy data. Second, the ends of the ridge lines appear to correspond accurately with the first swell energy observed in the data, as is the extension to lower frequencies where the dispersion pattern in the NAH model no longer is linear. Third, the low frequency swell energy observations appear to be rather noisy, making an objective model validation difficult.

A second event, originating around 0000 UTC on the 11th can be distinguished clearly in the NAH model at buoys 41001 and 44018 (Figs. 5.1c and 5.2c, crest line marked as 'D'). There is some indication of this swell system for buoy location 41012 (Fig. 5.3c), but the corresponding ridge line could not be estimated objectively from the local maxima in $F(f;t)$ due to an apparent merging with the previous event (line C). For buoy 41001, the occurrence of this system in the buoy data will be discussed in more detail below. For buoy 44018 (Fig. 5.2a), the event in the NAH model data can be identified in the buoy data within the same constraints as discussed above for event C.

A third event, originating on the 13th, can be distinguished in the NAH model at buoy 44018 (Fig. 5.2c, crest line marked as 'E'), and is also at least qualitatively identified in the buoy data (Fig. 5.2a). In data from the other two buoys, this event seems to have merged with the period of indistinguishable swells with a period of about 14 s, as discussed above.

So far, the assessment of wave conditions in the first swell period has been based on results of the NAH model, because this model more clearly identifies individual swell fields than the buoy data. The exception is the event marked 'F' observed at buoy 41001 (Fig. 5.1a), which does not appear in the NAH or WNA models. This event corresponds to the missed peak in the significant wave heights on the 15th in Fig. 4.4a. A ridge line analysis for this event suggests it originates around 1200 UTC the 13th. This is at the center of the period in which the GFDL winds systematically underestimated the wind speeds of Isabel (see Fig. 3.2a). A comparison with event D at this buoy location, suggests that event D represents the higher frequency edge of the observed event F, in particular for periods just following the end of ridge line D (that is, when the ridge starts to curve). The combination of the information from events D and F thus suggests that the observed event F corresponds to a swell field generated while Isabel was a category 5 hurricane. At this time, the GFDL model underestimated wind speeds, so that the NAH model could not properly generate the corresponding swell fields.

It is possible to identify other minor ridge lines in the NAH swell data for the first swell period, However, they do do not add insight to the present discussion, and are therefore not considered here. Furthermore, data before the 12th is not associated with Isabel, and will not be discussed here. These days are not

included in earlier plots with buoy data, but this time range is necessary here to track the generation time of individual swell fields.

6 Discussion

The present paper reviews the performance of NCEP's WNA and NAH regional wind wave models for hurricane Isabel from September 6 through 19, 2003. These two wave models are driven with winds from NCEP's GFS model, and with a blend of the GFS and high resolution GFDL winds near Isabel, respectively. Wind fields for both models have been compared to 25 independent surface wind analyses performed by AOML/HRD. The wave models have been validated with wave height and spectral data from 15 NDBC buoys, and with altimeter wave height data from the Jason-1 satellite. The later data included 4 four passes through or near the eye of Isabel, and many additional tracks with wave fields that are dominated by swells from Isabel. Thus a rich data set is available to validate these wave models for hurricane Isabel.

According to advisories from TPC, Isabel became a category 1 hurricane on September 7. From the 11th through the 15th, Isabel was a category 5 hurricane. After this, Isabel's size increased and strength diminished. Isabel was a category 2 hurricane for several days before landfall on the 19th. Validation data from AOML are available starting on the 11th. Our discussion will first focus on analyzed (hindcast) wind fields, using results presented in Figs. 3.1 through 3.3.

The GFDL winds as used in the NAH wave model briefly overestimate Isabel's intensity on the 11th, but generally underestimate maximum wind speeds when Isabel is a class 5 hurricane. Simultaneously, the GFDL winds provide realistic spatial scales of Isabel's wind fields. When Isabel starts to weaken, the GFDL wind intensities appear to be excellent, but the spatial scales of the wind fields appear somewhat under estimated. Under estimation of wind speed away from the area of maximum winds was observed in the GFDL model for hurricane Lili in Chao et al. (2004). For Isabel, these deficiencies appear much smaller than for Lili. This may be due to anomalous behavior of the GFDL model for Lili, or due to improvements made to the GFDL model before the 2003 Atlantic hurricane season.

The GFS winds as used in the WNA model severely underestimate Isabel's wind speeds when Isabel is a category 5 hurricane, and do not properly represent the structure of the wind fields. When Isabel starts to weaken and becomes larger, the GFS winds become more realistic in strength and structure. The last few days before landfall, the GFS maximum wind speeds are slightly low while the structure of Isabel is very well represented.

Forecast wind fields from the GFS and GFDL models show moderate track errors up to the 72 h forecast, as illustrated in Fig. 3.3. The corresponding errors for maximum wind speeds as presented in Fig. 3.2 suggest a systematic underestimation of the maximum wind speeds in the forecast. These errors are particularly large when Isabel is most intense, and they diminish as Isabel nears the coast (see Fig. 3.2). Timing errors in the tracks also also appear moderate

near the coast, as is illustrated in Figs. 4.8, 4.9 and 4.10.

Wave heights from the NAH and WNA models have been validated using buoy and altimeter data. Again, our attention is first focused on hindcasts. In broad lines the accuracy of the wave models can be traced to the quality of the wind fields, as will be discussed below.

On the 11th, waves hindcasts from the NAH model are too high when compared to the altimeter data. This corresponds to a period when the GFDL wind fields appear too strong compared to the AOML analysis. Against all other altimeter data, the hindcast wave heights from the NAH model appear very accurate. The reproduction of the eye structure in the wave heights on the 17th is particularly impressive (third set of panels in Fig. 4.1). On the 15th and 16th, the NAH model does not produce early swell arrivals at most buoy locations particularly well (Figs. 4.4 through 4.7). The MBU plot for buoy 41001 (Fig. 5.1) indicates that these swell fields were generated when Isabel was a category 5 hurricane. During this period, the GFDL wind speeds underestimated the strength of Isabel (Fig. 3.2), which at least qualitatively explains the underestimation of these swell fields in the NAH model.

Wave hindcasts from the WNA model severely underestimate observations when Isabel is a category 5 hurricane (Fig. 4.1 to panels), as would be expected from the severe underestimation of the corresponding wind speeds (Fig. 3.2). The corresponding swell fields are generally under estimated as is evident in the swell dominated altimeter data (Fig. 4.2), and to a lesser extent in the buoy data for the 12th through the 16th (see Figs. 4.4 through 4.7). Near landfall, the wave heights produced by the WNA model become much more realistic (Fig. 4.1 lower panels and Figs. 4.4 through 4.7), and are similar to the results of the NAH model. Interestingly, the WNA model appears to be sending too much wave energy in easterly directions in the latter time period (Fig. 4.2 bottom panels). This behavior was not expected and cannot readily be explained. However, because it does not appear in the results of the NAH model, it appears to be related to details of the near surface circulation of Isabel in the GFS model.

So far, we have discussed hindcasts of wave heights. Although this is important to address the accuracy of model results, the actual forecasts accuracy is what is crucial for providing forecast guidance at NCEP. The forecast accuracy is addressed here with the wave height envelopes for the 0-72h forecasts for the NAH model for selected buoys in Fig. 4.8, and with example forecast wave height fields for the NAH and WNA models in Figs. 4.9 and 4.10, respectively. The former figure shows narrow envelopes of forecast wave heights, similar in width to the 95% confidence interval of wave height observations from buoys. The latter figures suggest that the errors are mostly related to timing errors, with Isabel moving too fast in the NAH model, and too slow in the WNA model. In general, however, it is clear that both wave models provided excellent guidance up to the 72 H forecast horizon of the NAH model, with the NAH model being significantly

more accurate with respect to swell forecasts.

The MBU plots of Figs. 5.1 through 5.3 have not been commonly used in recent literature. Exceptions are Melo and Alves (1995), Wingeart et al. (2001) and Chao et al. (2004). Such plots however, are a concise way of presenting detailed spectral information. They identify individual swell fields that coexist, but which would go undetected when using a single peak period T_p in the validation. MBU plots are particularly useful for analysis of swell fields in model results, due to the capability of models to consistently track swell fields with low energy. In observational data, sampling errors and signal to noise ratios contaminate the signature for long swells. This somewhat limits the usefulness of such plots for routinely observed spectra. In the present study, the MBU plots proved helpful in tracking the sources of wave model errors.

Wave model results for Isabel were excellent, and many of its deficiencies can be attributed to deficiencies in the wind fields used as forcing in these models. There are nevertheless several wave model issues that leave room for improvement, or invite further discussion. Below we will discuss the following issues in more detail: (i) wave model behavior in shallow water, (ii) prediction of extreme wave conditions, (iii) wave-current interactions, (iv) predictability of wave conditions, and (v) numerical issues. These issues all have a direct impact on the quality of the numerical wave guidance, and represent possible avenues of further research.

The most obvious shortcoming of both wave models is the over estimation of the wave heights H_s in shallow water on the shelf for buoy 41008 (Fig. 4.5a), and to a lesser extend at buoy 41012 (Fig. 4.5b). This behavior appears consistent in this shelf region according to the Jason-1 altimeter data presented in Fig. 4.3. Tentatively, this can be attributed to inadequate modeling of shallow water processes such as surf zone physics, refraction, and bottom friction.

Surf zone physics are not included in WAVEWATCH III. However, the observed maximum wave height to depth ratio $(H_s/d)_{\max} < 0.2$ for both buoys. Within the surf zone $H_s/d \approx 0.6$. This suggests that both buoys are well outside the surf zone at all times, and that the absence of surf zone physics in the model is not an issue.

Refraction can lead to local focusing and shadow areas. If this leads to significant variations in the local wave heights, significant spatial variability of wave heights would be expected in the near shore Jason-1 data in Fig. 4.3. Similarly, temporal variability might be expected in time series of wave heights observed at buoys, because shifts in the direction of incoming swells will result in a spatial shift of focusing and shadow areas. Because such spatial and temporal variability is not observed in the altimeter or buoy data, it is not likely that the model deficiencies for buoys 41008 and 41012 are cause by refraction.

The bottom friction coefficient as used in the wave models ($\Gamma = -0.019\ \mathrm{m^2 s^{-3}}$, Table 2.1) is smaller by a factor of 2 to 4 than traditionally recommended values

(e.g., Hasselmann et al., 1973; Bouws and Komen, 1983). This value was adopted to properly describe the extremely smooth shallow water areas in the Gulf of Mexico[9]. The bottom at the Atlantic shelf is, due to its exposure to extreme swell conditions, likely to be rougher than the bottom in the Gulf of Mexico. The bottom friction setting in the model therefore are expected to result in an underestimation of the energy loss due to bottom friction at the Atlantic shelf. This appears to be the most likely explanation for the overestimation of the wave heights at buoys 41008 and 41012.

The second issue that requires additional discussion is the prediction of extreme wave conditions in extreme wind conditions. Buoys rarely observe (and survive) such conditions. Altimeter data also proves sensitive to drop-outs in hurricane wave conditions (e.g., Fig. 4.1). This makes assessment of model performance in the most extreme conditions difficult. Nevertheless, some interesting observations can be made from the present data.

The altimeter track through the eye of Isabel on the 13th (Fig. 4.1b) occurs in a period in which the model wind in the NAH model appears to be under estimated (Fig. 3.2), yet the corresponding wave heights do not appear to be under estimated. It can also be observed that near landfall the NAH winds appear to be of proper intensity, but cover an areas that appears to be too small, whereas the WNA winds appear to have the proper spatial scales, yet appear to be too weak (Figs. 3.1 and 3.2). However, the corresponding wave heights near Isabel do not appear to be under estimated (Fig. 4.4) as would be expected.

Both observations suggest that wave growth in hurricane conditions is too rapid in the wave model. This can tentatively be explained by recent observations of surface stresses in hurricane conditions. Wave growth rates scale with the corresponding friction velocity or drag coefficient (Tolman and Chalikov, 1996). Common relations for the drag coefficient are based on observations in a narrow range of moderate wind speeds. Recent observations and theories (e.g., Powell et al., 2003; Moon et al., 2004) suggest that extrapolation of these relations to extreme conditions over estimate drag coefficients and stresses, and would hence over estimate wave growth rates. This represents a potential deficiency in the wave model physics.

The third issue that deserves further attention is the effect of wave-current interactions, which appear to be present in the observations from buoy 44018 (Figs. 4.7c and 5.2), and which also appear occasionally in the observations from several other buoys. Part of the observed wave current interactions can be attributed to the fact that a moored buoy observes frequencies in a fixed frame of reference. For a wave component with a given wavenumber vector $\boldsymbol{k}$ this so-called absolute frequency $\omega = 2\pi f_a$ differs from the intrinsic frequency $\sigma = 2\pi f$ according to the dispersion and Doppler relations

[9] See http://polar.ncep.noaa.gov/waves/mod/bot1/

$$\sigma^2 = gk \tanh kd \quad , \tag{6.1}$$

$$\omega = \sigma + \boldsymbol{k} \cdot \boldsymbol{U} \quad , \tag{6.2}$$

where $k = ||\boldsymbol{k}||$, d is the mean water depth and $\boldsymbol{U}$ is the mean current velocity. The spectrum $F(f, \theta)$ is defined relative to the mean motion of the water mass. The spectrum $F(f_a, \theta)$, however, is observed with a moored buoy. The spectra are related with a Jacobean transformation

$$F(f_a, \theta) = \left(1 + \frac{\boldsymbol{k} \cdot \boldsymbol{U}}{kc_g}\right)^{-1} F(f, \theta) \quad , \tag{6.3}$$

where $c_g = \partial\sigma/\partial k$ is the group velocity.

In idealized quasi-homogeneous currents, as representative for waves on tides away from bathymetric features (Tolman, 1990), the spectrum $F(f, \theta)$ remains invariant, and the observed spectrum follows directly from the local current and Eqs. (6.1) through (6.3). For slowly varying currents, the same relation holds true in the equilibrium range of the spectrum (Tolman, 1991a,b). Because $F(f)$ rapidly decreases with f in this part of the spectrum, and because U/c_g then is generally large, tidal modulations in this part of the spectrum $F(f_a)$ as observed by buoys is generally large. Furthermore, the modulation tends to increase with increasing f_a, as can be observed in Fig. 5.2. This might suggest that at least some of the wave-current interactions can be added to the model by post processing, that is, by computing $F(f_a)$ from $F(f)$ given the local current $\boldsymbol{U}$ and depth d only. However, the corresponding transformation (6.3) conserves wave energy and hence wave heights. Figure 4.7c indicates that the wave height also appears to be subject to tidal modulation. This implies that full wave current interactions, including effects of current refraction and momentum exchange between waves and currents need to be considered in order to properly model the apparent wave current interactions observed at buoy 44018.

Wave current interactions also appear to occur in the Gulf Stream region in Fig. 4.3. Such interactions are likely due to swells or wind seas trapped in the Gulf Stream (for a review, see Holthuijsen and Tolman, 1991). Proper modeling of these effects also requires full implementation of wave current interactions in the model.

The fourth issue to be discussed in more detail is the predictability of hurricane waves. Conventionally, wave models are forced with relatively smooth and slowly varying wind fields. Combined with the fact that hyperbolic equations of a wave model represent a forced and damped physical system, chaotic behavior is generally not expected. Predictability is therefore generally not considered to be a relevant issue in wave modeling. However, altimeter data away from the center of Isabel as presented in Fig. 4.2 show a distinct variability on small to moderate spatial scales. Moreover, animation of hourly modeled wind and wave

height fields of Isabel (not presented here), indicate that the typical 'pulsating' nature of modeled hurricane wind field is also evident in the wave height fields. This suggests that hurricane wave conditions are more chaotic than more moderate wave conditions, and hence may have a more limited predictability. This also raises the question if sharp individual swell signatures as identified in the model results in the MBU plots (Figs. 5.1 through 5.3) should be considered as purely deterministic model results, or as a (partially) random realization of chaotic aspects of the hurricane wind and wave fields.

Finally, two numerical issues deserve additional attention. First, buoy 44018 (Fig. 4.7c), and to a lesser extend buoys 44009 (Fig. 4.6a), 44008 and 44011 (Figs. 4.7a,b), display noise in the wave heights H_s from the NAH model with a period of two times the overall time step of the model. Normally, such noise is associated with numerical instabilities in the model. For WAVEWATCH III, it is suspected that this is due to the fact that the order of the spatial and refraction computations are alternated per time step for numerical accuracy. For relatively well resolved fields, this indeed increases numerical accuracy. For poorly resolved fields, however, this introduced noise with a period of $2\Delta t$. Second, several panels in Figs. 4.1 and 4.2 appear to display the so-called Garden Sprinkler Effect (GSE), which points to a (moderate) disintegration of swell fields in discrete swell fields corresponding to the discretization of $F(f, \theta)$ (Booij and Holthuijsen, 1987; Tolman, 2002b). Both issues can be addressed by minor tuning of existing numerical methods in the WAVEWATCH III model. We intend to investigate this in some more detail using Isabel as a test case, and we intend to implement adjustments as justified by such tests before the 2004 Atlantic hurricane season.

7 Conclusions

The present study addresses the accuracy of two operational wave models of the National Centers for Environmental Prediction (NCEP) for hurricane Isabel. With many independent wind analyses, and wave observations from the Jason-1 altimeter and 15 NDBC buoys, a rich validation data set is available. It is shown that the model specifically developed for hurricane wave prediction (NAH) generally outperforms the 'generic' WNA model, particularly when Isabel was a relatively small but intense category 5 hurricane. Both models showed excellent forecasts for Isabel near landfall for the 72 h forecast horizon of the NAH model, and for several more days for the WNA model. Most model deficiencies are shown to be related to deficiencies in the wind fields used to force the two models. However, it also appears that there is still room for improvement in the underlying generic wave model with respect to (i) wave model behavior in shallow water, in particular on the southern Atlantic shelf (ii) physical parameterizations for extreme wind conditions, (iii) inclusion of wave-current interactions, and (iv) several numerical issues. The present results also indicate that there may be limits to the predictability of hurricane swells. Such limits have not been encountered in wave modeling before, to the knowledge of the present authors.

This page is intentionally left blank.

References

Barber, N. F. and F. Ursell, 1947: The generation and propagation of ocean waves and swell. *Trans. Roy. Soc. London*, **240(A)**, 527–560.

Booij, N. and L. H. Holthuijsen, 1987: Propagation of ocean waves in discrete spectral wave models. *J. Comput. Physics*, **68**, 307–326.

Bouws, E. and G. J. Komen, 1983: On the balance between growth and dissipation in an extreme depth-limited wind-sea in the southern north sea. *J. Phys. Oceanogr.*, **13**, 1653–1658.

Caplan, P., J. Derber, W. Gemmill, S.-Y. Hong, H.-L. Pan and D. Parish, 1997: Changes to the 1995 NCEP operational medium-range forecast model analysis/forecast system. *Wea. Forecasting*, **12**, 581–594.

Chao, Y. Y., L. D. Burroughs and H. L. Tolman, 2003a: The North Atlantic Hurricane wind wave forecasting system (NAH). Technical Procedures Bulletin 478, NOAA/NWS, online[1].

Chao, Y. Y., L. D. Burroughs and H. L. Tolman, 2003b: Wave forecasting for the Western North Atlantic and adjacent waters. Technical Procedures Bulletin 495, NOAA/NWS, online[2].

Chao, Y. Y. and H. L. Tolman, 2000: Numerical experiments on predicting hurricane generated wind waves. in *Preprints 6th international workshop on wave hindcasting and forecasting*, pp. 167–179. Environment Canada.

Chao, Y. Y. and H. L. Tolman, 2001: Specification of hurricane wind fields for ocean wave prediction. in B. L. Edge and J. M. Hemsley, editors, *Ocean Wave Measurement and Analysis*, pp. 671–679. ASCE.

Chao, Y. Y., H. L. Tolman and J. H. G. M. Alves, 2004: A system for predicting hurricane-generated wind waves in the north Atlantic Ocean. In Preparation.

Chen, H. S., L. D. Burroughs and H. L. Tolman, 2003: Ocean surface waves. Technical Procedures Bulletin 494, NOAA/NWS, online[3].

Donelan, M. and W. J. Pierson, 1983: The sampling variability of estimates of spectra of wind-generated gravity waves. *J. Geophys. Res.*, **88**, 4381–4392.

Earle, M. D., 2003: Nondirectional and directional wave data analysis procedures. Technical Document 03–01, NOAA/NWS/NDBC.

Grumbine, R. W., 1996: Automated passive microwave sea ice concentration analysis at NCEP. Tech. Note 120, NOAA/NWS/NCEP/OMB, 13 pp.

Hasselmann, K., T. P. Barnett, E. Bouws, H. Carlson, D. E. Cartwright, K. Enke, J. A. Ewing, H. Gienapp, D. E. Hasselmann, P. Kruseman, A. Meerburg, P. Mueller, D. J. Olbers, K. Richter, W. Sell and H. Walden, 1973: Measurements of wind-wave growth and swell decay during the Joint North Sea Wave Project (JONSWAP). *Ergaenzungsheft zur Deutschen Hydrographischen*

[1] http://polar.ncep.noaa.gov/mmab/tpbs/tpb478/tpb478.htm

[2] http://polar.ncep.noaa.gov/mmab/tpbs/tpb495/tpb495.htm

[3] http://polar.ncep.noaa.gov/mmab/tpbs/tpb494/tpb494.htm

Zeitschrift, Reihe A(8), **12**, 95 pp.

Holthuijsen, L. H. and H. L. Tolman, 1991: Effects of the gulf stream on ocean waves. *J. Geophys. Res.*, **96**, 12755–12771.

Melo, E. and J. H. G. M. Alves, 1995: Instrumental confirmation of the arrival of long-crested swell to the Ceara coast. in *Proc. 4st Int. Conf. Coastal Port Eng. Devlop. Countries, Rio de Janeiro, Brazil*, pp. 1984–1996.

Moon, I. J., T. Hara, I. G. S. E. Belcher and H. L. Tolman, 2004: Effect of surface waves on air-sea momentum exchange: I. Effect of mature and growing seas. Submitted.

Moorthi, S., H. Pan and P. Caplan, 2001: Changes to the 2001 NCEP operational MRF/AVN global analysis/forecast system. Technical Procedures Bulletin 484, NOAA/NWS, online[4].

Munk, W. H., 1947: Tracking storms by forerunners of swell. *J. Meteorol.*, **4**, 45–57.

Powell, M. D., S. H. Houston, L. R. Amat and N. Morisseau-Leroy, 1998: The HRD real-time hurricane wind analysis system. *J. Wind Engineer. and Indust. Aerodyn.*, **77–78**, 53–64.

Powell, M. D., S. H. Houston and T. A. Reinhold, 1996: Hurricane Andrew's landfall in south Florida. Part I: standardizing measurements for documentation of surface wind fields. *Wea. Forecasting*, **11**, 304–328.

Powell, M. D., P. J. Vickery and T. A. Reinhold, 2003: Reduced drag coefficient for high wind speeds in tropical cyclones. *Nature*, **442**, 279–283.

Snodgrass, F. E., G. W. Groves, K. F. Hasselmann, G. R. Miller, W. H. Munk and W. H. Powers, 1966: Propagation of swell across the pacific. *Trans. Roy. Soc. London*, **A 259**, 431–497.

Tolman, H. L., 1990: The influence of unsteady depths and currents of tides on wind wave propagation in shelf seas. *J. Phys. Oceanogr.*, **20**, 1166–1174.

Tolman, H. L., 1991a: Effects of tides and storm surges on north sea wind waves. *J. Phys. Oceanogr.*, **21**, 766–781.

Tolman, H. L., 1991b: A third-generation model for wind waves on slowly varying, unsteady and inhomogeneous depths and currents. *J. Phys. Oceanogr.*, **21**, 782–797.

Tolman, H. L., 2002a: The 2002 release of WAVEWATCH III. in *Preprints 7th international workshop on wave hindcasting and forecasting*, pp. 188–197. Environment Canada.

Tolman, H. L., 2002b: Alleviating the garden sprinkler effect in wind wave models. *Ocean Mod.*, **4**, 269–289.

Tolman, H. L., 2002c: User manual and system documentation of WAVEWATCH III version 2.22. Tech. Note 222, NOAA/NWS/NCEP/MMAB, 133 pp.

Tolman, H. L., B. Balasubramaniyan, L. D. Burroughs, D. V. Chalikov, Y. Y. Chao, H. S. Chen and V. M. Gerald, 2002: Development and implementation

[4] http://www.nws.noaa.gov/om/tpb/

of wind generated ocean surface wave models at NCEP. *Wea. Forecasting*, **17**, 311–333.

Tolman, H. L. and D. V. Chalikov, 1996: Source terms in a third-generation wind-wave model. *J. Phys. Oceanogr.*, **26**, 2497–2518.

Wingeart, K. M., W. C. O'Reilly, T. H. C. Herbers, P. A. Wittmann, R. E. Jenssen and H. L. Tolman, 2001: Validation of operational global wave prediction models with spectral buoy data. in B. L. Edge and J. M. Hemsley, editors, *Ocean Wave Measurement and Analysis*, pp. 590–599. ASCE.

Young, I. R., 1986: Probability distribution of spectral integrals. *J. of Waterway, Port, Coastal and Ocean Eng.*, **112**, 338–341.